UNIVERSITÀ
DEGLI STUDI
DI PADOVA

DIPARTIMENTO
DI INGEGNERIA
DELL'INFORMAZIONE

DIPARTIMENTO DI INGEGNERIA DELL'INFORMAZIONE

CORSO DI LAUREA MAGISTRALE IN INEGEGNERIA ELETTRONICA

"TIME OPTIMAL CURRENT AND SPEED CONTROL OF A IPM SM"

Relatore: Prof. Nicola Bianchi

Laureando/a: Riccardo Dall'Alba

ANNO ACCADEMICO 2022 – 2023

Data di laurea 10 luglio 2023

To my family.

Contents

Abstract

In the present days, the demand for systems with extremely fast large-signal torque responses is increasing. Emerging applications, like electrical test rigs for automotive, can't be implemented effectively with PID-like controllers. In fact these types of controllers show good behaviour in quasi steady state conditions, but perform poorly under great variations of torque, further more if the current regulators are saturated. PID controllers aren't optimized to work in voltage saturation conditions.
A solution to the issue posed by these system in need of a fast response, has already been proposed by Doc. Matteo Tommasini in his PhD thesis: "Innovative control algorithms for electric drives", in which the author presents two new strategies for fast motor control, the Time Optimal Current and Torque Controls ($toCc$ and $toTc$). In his paper Tommasini uses the Optimal Control theory to derive both controls' strategies. The followed procedure will be also presented in this Master Thesis, first on the same IPM motor used in Tommasini's paper, and then it will be used together with a speed control.

Sommario

Al giorno d'oggi, la domanda di sistemi con risposte di coppia estremamente veloci per segnali di grandi dimensioni è in aumento. Le applicazioni emergenti, come i banchi di prova elettrici per il settore automobilistico, non possono essere implementate in modo efficace con controller di tipo PID. Infatti questi tipi di controllori mostrano un buon comportamento in condizioni quasi stazionarie, ma si comportano male con grandi variazioni di coppia, tanto più se i regolatori di corrente sono saturi. I controller PID non sono ottimizzati per funzionare in condizioni di saturazione della tensione.
Una soluzione al problema posto da questi sistemi che necessitano di una rapida risposta, è già stata proposta dal doc. Matteo Tommasini nella sua tesi di dottorato: "Algoritmi di controllo innovativi per azionamenti elettrici", in cui l'autore presenta due nuove strategie per il controllo di motori veloci, i controlli Time Optimal Current e Torque ($toCc$ e $toTc$). Nel suo articolo Tommasini utilizza la teoria del controllo ottimo per derivare le strategie di entrambi i controlli. La procedura seguita sarà presentata anche in questa tesi di laurea, prima sullo stesso motore IPM utilizzato nell'articolo di Tommasini, e poi verrà utilizzato insieme a un controllo di velocità.

Chapter 1

Introduction

On the first part of this thesis it will be summarized the procedure done by Dr. Matteo Tommasini in his PhD Thesis to implement the time optimal current control on an Internal Permanent Magnet Synchronous Motor. One the second part instead it will be build a PI speed regulator for the same motor which uses the *toCc* in the current loop control.
In this chapter it will be presented the motor used in the PhD thesis, together with a brief description of the convention used to describe the state equations of the motor.
In the second chapter it will be presented the Maximum principle Theorem, used to derive the Time Optimal Current Control (*toCc*), along with the control implemented on Matlab and Simulink.

1.1 Motor Specs.

In order to better understand the methodology behind the time optimal control, it has been reproduce the work done in Tommasini's thesis, using the same motor typology and characteristics. In the table below it has been reported the parameters of the motor used.

Parameter	Value
Rated Voltage	230 V
Rated Standstill Current(100K)	3.9 A
Rated Standstill Torque(100K)	5.1 Nm
Phase Resistance($20°C$)	4.85 Ω
Connection	Y
Pole Number	4
Speed(max)	4000 rpm
Base Speed (motor)	1880 rpm
Base Speed (generator)	2540 rpm
id max Torque	-4.04 A_{pk}
iq max Torque	3.75 A_{pk}
PM flux linkage	0.194 Vs
d-axis inductance (unsaturated)	30 mH
q-axis inductance (unsaturated)	153 mH

Further more (differently to the reference thesis) it has been assumed the IPMSMotor to be ideal, so its parameters are considered constant (and in particular the inductance L_q). As a result of that some of the parameters in the table could differ from the ones found in the simulations.

1.2 Used Conventions and Motor model

To obtain the electrical quantities values along the conventional reference frames (abc, $\alpha\beta$, dq) it has been used the *Peak Convention*. As a result given an arbitrary electrical quantity x_a, x_b, x_c in the abc-frame, the passage to the $\alpha\beta$-frame is carried out by means of the equations:

$$\begin{cases} x_\alpha = \frac{2}{3}\left(x_a - \frac{1}{2}x_b - \frac{1}{2}x_c\right) \\ x_\beta = \frac{2}{3}\left(\frac{\sqrt{3}}{2}x_b - \frac{\sqrt{3}}{2}x_c\right) \end{cases}$$

defining $x_{\alpha\beta} = x_\alpha + jx_\beta$, on the stationary $\alpha\beta$-frame. The passage between stationary frame and the rotating dq-frame becomes:

$$x_{dq} = x_{\alpha\beta}e^{-j\theta_{me}}$$

with θ_{me} being the electromechanical angle of the rotor with respect the stationary $\alpha\beta$-frame.

Given the electrical quantities in the dq-frame it is now possible to give the state equations of IPMSM. In this paper the control and motor will be studied mostly in the dq-frame. In this plane the state equations are:

$$\begin{cases} u_d = Ri_d + \dfrac{d\lambda_d}{dt} - w_{me}\lambda_q \\ u_q = Ri_q + \dfrac{\lambda_q}{dt} + w_{me}\lambda_d \end{cases} \tag{1.1}$$

where:

R	phase resistance
u_d, u_q	voltage along d- and q-axis;
i_d, i_q	current along d- amd q-axis;
λ_d, λ_q	flux linkage along d- and q-axis;
$w_{me} = p \cdot w_m$	electromechanical rotor velocity (p pole pairs, w_m mechanical rotor speed).

the state equations (1.1) can also be expressed differently by replacing the flux linkage with its explicit formula:

$$\begin{cases} \lambda_d = L_d i_d + \Lambda_m \\ \lambda_q = L_q i_q \end{cases}$$

by carrying out said replacement the system (1.1) becomes:

$$\begin{cases} u_d = Ri_d + \dfrac{di_d}{dt}L_d - w_{me}L_q i_q \\ u_q = Ri_q + \dfrac{di_q}{dt}L_q + w_{me}(L_d i_d + \Lambda_m) \end{cases} \tag{1.2}$$

Both equations (1.1) and (1.2) will be used during the realization of the *toCc* and PI regulators.
An other equation useful to the realization of the IPMSM control is the Torque one, which, like system (1.1), can be expressed in two ways:

$$T = \frac{3}{2}p\left(\lambda_d i_q - \lambda_q i_d\right) \tag{1.3}$$

$$T = \frac{3}{2}pi_q\left[\left(L_d - L_q\right)i_d + \Lambda_m\right] \tag{1.4}$$

Chapter 2

Optimal Control Theory

The *"Optimal Control"* deals with the problem of finding a control law for a given system such that a certain optimality criterion is achieved. A control problem includes a cost functional that is a function of state and control variables. An optimal control is a set of differential equations describing the paths of the control variables that minimize the cost function. If the function to minimize is time than the control takes name of *"Time Optimal Control"*. In this chapter will be presented the *Maximum Principle* which will then be applied to the model of the IPMSM to obtain its *Time Optimal Current Control* (*toCc*)..

2.1 Maximum Principle for Time Optimality

Let's now define the variables introduced in the *Maximum Principle* definition:

- $(x_1, \ldots, x_r) = \boldsymbol{x} \in \boldsymbol{X}$ are the variables which characterize the process, and $\boldsymbol{X}$ is the set of space with coordinates $x_1, \ldots, x_n$, to which $\boldsymbol{x}$ belongs to;
- $(u_1, \ldots, u_r) = \boldsymbol{u} \in \boldsymbol{U}$ indicates the control parameters which determine the course of the process, while $\boldsymbol{U}$ is the *control region*, a set of space with coordinates $u_1, \ldots, u_r$, to which $\boldsymbol{u}$ belongs to.

Both sets $\boldsymbol{X}$ and $\boldsymbol{U}$ are usually closed and bounded by physical limitations of the system and control parameters (e.g., in electric motor drives, $\boldsymbol{X}$ could be bounded by specific current limits, while $\boldsymbol{U}$ could be limited by the supply voltage of the motor). Let's now consider a process described by an

autonomous system of ordinary differential equations:

$$\frac{dx_i}{dt} = f_i(x_1, \ldots, x_n, u_1, \ldots, u_r), \quad i = 1, \ldots, n \tag{2.1}$$

of which given the initial values

$$x_i(t_0) = \boldsymbol{x}_0, \quad i = 1, \ldots, n$$

and the control parameters in a certain time interval $t_0 \leq t \leq t_1$:

$$u_j = u_j(t) = \boldsymbol{u}(t), \quad j = 1, \ldots, r$$

the solution of equation (2.1) is uniquely determined. Let's consider also the integral functional:

$$J = \int_{t_0}^{t_1} f_0(\boldsymbol{x}, \boldsymbol{u}) dt \tag{2.2}$$

where $f_0(\boldsymbol{x}, \boldsymbol{u})$ is a given function, defined and continuos together with its partial derivatives $\partial f_0 / \partial x_i$, $i = 1, \ldots, n$, on all $\boldsymbol{X} \times \boldsymbol{U}$. The functional J takes on a defined value for each control $\boldsymbol{u}(t)$.
The objective is to find the control set $\boldsymbol{u}(t)$ that minimize the value J, in particular when the function $f_0(\boldsymbol{x}, \boldsymbol{u}) = 1$, which leaves $J = t_1 - t_0$ and the problem takes name of *time-optimal*. In such case the *admissible control* $\boldsymbol{u}(t)$ (defined as a control $\boldsymbol{u} \in \boldsymbol{U}$ which is continuos in the time interval considered, with only first kind discontinuities allowed), which minimize the time transition from $\boldsymbol{x}(t_0) = \boldsymbol{x}_0$ to $\boldsymbol{x}(t_1) = \boldsymbol{x}_1$ is called *optimal control*. The corresponding trajectory $\boldsymbol{x}(t)$ is called *optimal trajectory*.
In order to understand the *Maximum Principle*, it is useful to define a new coordinate x_0 such that:

$$\frac{dx_0}{dt} = f_0(\boldsymbol{x}, \boldsymbol{u}). \tag{2.3}$$

Introducing $\tilde{\boldsymbol{x}} = (x_0, x_1, \ldots, x_n) \in \tilde{\boldsymbol{X}}$ we can write:

$$\frac{d\tilde{\boldsymbol{x}}}{dt} = \tilde{\mathbf{f}}(\boldsymbol{x}, \boldsymbol{u}) = (f_0(\boldsymbol{x}, \boldsymbol{u}), f_1(\boldsymbol{x}, \boldsymbol{u}), \ldots, f_n(\boldsymbol{x}, \boldsymbol{u})) \tag{2.4}$$

Defining $\tilde{\boldsymbol{x}}_{\mathbf{o}} = (0, \boldsymbol{x}_{\mathbf{o}})$, the solution of the system (2.4) with initial condition $\boldsymbol{x}_{\mathbf{o}}$ at time t_0 and final condition x_1 at time t_1 becomes

$$\begin{cases} x_0 = \displaystyle\int_{t_0}^{t} f_0(\boldsymbol{x}(\tau), \mathbf{u}(\tau)) d\tau \\ \boldsymbol{x} = \boldsymbol{x}(t) \end{cases} \tag{2.5}$$

for $t = t_1$ it results

$$x_0 = J, \quad \boldsymbol{x} = \boldsymbol{x}_1.$$

Let's now define an auxiliary system as:

$$\begin{cases} \dfrac{d\psi_0}{dt} = -\dfrac{\partial f_0(\boldsymbol{x}, \boldsymbol{u})}{\partial x_0}\psi_0 - \cdots - \dfrac{\partial f_n(\boldsymbol{x}, \boldsymbol{u})}{\partial x_0}\psi_n \\ \quad \vdots \\ \dfrac{d\psi_n}{dt} = -\dfrac{\partial f_0(\boldsymbol{x}, \boldsymbol{u})}{\partial x_n}\psi_0 - \cdots - \dfrac{\partial f_n(\boldsymbol{x}, \boldsymbol{u})}{\partial x_n}\psi_n \end{cases} \tag{2.6}$$

and let's also define the function $\mathcal{H}$ as follows:

$$\mathcal{H}(\tilde{\boldsymbol{\psi}}, \boldsymbol{x}, \boldsymbol{u}) = \mathcal{H}(\psi_0, \ldots, \psi_n, x_1, \ldots, x_n, u_1, \ldots, u_r) = \sum_{\alpha=0}^{n} \psi_\alpha f_\alpha(\boldsymbol{x}, \mathbf{u}). \tag{2.7}$$

By observation of the systems (2.6) and (2.7) it is possible to extrapolate a new system:

$$\begin{cases} \dfrac{dx_i}{dt} = \dfrac{\partial \mathcal{H}}{\partial \psi_i} & i = 0, 1, \ldots, n \\ \dfrac{d\psi_i}{dt} = -\dfrac{\partial \mathcal{H}}{\partial x_i} & i = 0, 1, \ldots, n \end{cases} \tag{2.8}$$

By reasoning in the time-optimal problem it is possible to simplify the equations by remembering that in such case $f_0(\boldsymbol{x}, \mathbf{u}) = 1$. A new function $H(\boldsymbol{\psi}, \boldsymbol{x}, \boldsymbol{u})$ can be defined:

$$H(\boldsymbol{\psi}, \boldsymbol{x}, \boldsymbol{u}) = \mathcal{H}(\psi_1, \ldots, \psi_n, x_1, \ldots, x_n, u_1, \ldots, u_r) = \sum_{\nu=1}^{n} \psi_\nu f_\nu(\boldsymbol{x}, \mathbf{u}). \tag{2.9}$$

while the system (2.8) becomes:

$$\begin{cases} \dfrac{dx_i}{dt} = \dfrac{\partial H}{\partial \psi_i} & i = 1, \ldots, n \\ \dfrac{d\psi_i}{dt} = -\dfrac{\partial H}{\partial x_i} & i = 1, \ldots, n \end{cases} \tag{2.10}$$

By fixing the values of $\boldsymbol{\psi}$ and $\boldsymbol{x}$, H becomes function of $\boldsymbol{u}$. It is possible to denote the superior of such function as:

$$M(\boldsymbol{\psi}, \boldsymbol{x}) = \sup_{\boldsymbol{u} \in \boldsymbol{U}} H(\boldsymbol{\psi}, \boldsymbol{x}, \boldsymbol{u}). \tag{2.11}$$

The *Maximum Principle for Time Optimality* lays down the necessary conditions for time optimality and it is the following:

Let $\boldsymbol{u}(t)$, $t_0 \leq t \leq t_1$, be an admissible control which transfer the phase point from $\boldsymbol{x}_0$ to $\boldsymbol{x}_1$, and let $\boldsymbol{x}(t)$ be the corresponding trajectory, so that $\boldsymbol{x}(t_0) = \boldsymbol{x}_0$ and $\boldsymbol{x}(t_1) = \boldsymbol{x}_1$. In order that $\boldsymbol{u}(t)$ and $\boldsymbol{x}(t)$ be time optimal it is necessary that there exist a nonzero, continuos vector function $\boldsymbol{\psi}(t) = (\psi_1(t), \ldots, \psi_n(t))$ corresponding to $\boldsymbol{u}(t)$ and $\boldsymbol{x}(t)$ such that:

1. for all t, $t_0 \leq t \leq t_1$, the function $H(\boldsymbol{\psi}(t), \boldsymbol{x}(t), \boldsymbol{u})$ of the variable $\boldsymbol{u} \in \boldsymbol{U}$ attains its maximum at the point $\boldsymbol{u} = \boldsymbol{u}(t)$

$$H(\boldsymbol{\psi}(t), \boldsymbol{x}(t), \boldsymbol{u}(t)) = M(\boldsymbol{\psi}(t), \boldsymbol{x}(t)); \tag{2.12}$$

2. at the terminal time t_1 the relation

$$M(\boldsymbol{\psi}(t_1), \boldsymbol{x}(t_1)) \geq 0 \tag{2.13}$$

   is satisfied.

Further more, if $\boldsymbol{\psi}(t)$, $\boldsymbol{x}(t)$ and $\boldsymbol{u}(t)$ satisfy both condition 1 and the system (2.10), the time function $M(\boldsymbol{\psi}(t), \boldsymbol{x}(t))$ is constant. Thus (2.13) may be verified at any time t, $t_0 \leq t \leq t_1$, and not just at t_1.

2.2 Time Optimal Current Control Theory

In this section the *Maximum Principle* will be applied to a model of the IPMSM, firstly considering a circular voltage limit, then in the real case with an hexagonal one.
Since a current control is to be implemented it is known that the input of the system will be the current reference vector, while the output will be the voltage reference vector. The objective is to find the optimal voltage vector which minimize the time transfer from a known initial state to also known final condition. For simplicity the problem will be studied in the dq-reference frame, working with the flux linkage (the phase resistance R will be neglected).
Under such hypothesis the system (1.1) becomes:

$$\begin{bmatrix} \dot{\lambda}_d \\ \dot{\lambda}_q \end{bmatrix} = \begin{bmatrix} 0 & w_{me} \\ -w_{me} & 0 \end{bmatrix} \begin{bmatrix} \lambda_d \\ \lambda_q \end{bmatrix} + \begin{bmatrix} 1 & 0 \\ 0 & 1 \end{bmatrix} \begin{bmatrix} u_d \\ u_q \end{bmatrix} \tag{2.14}$$

or compacted:

$$\dot{\boldsymbol{\lambda}} = \boldsymbol{F}\boldsymbol{\lambda} + G\boldsymbol{u} \tag{2.15}$$

The time optimality problem becomes the following:

For the process described by the system of equations (2.14), find the optimal control $\boldsymbol{u} \in \boldsymbol{U}$ able to change the state of the process from $\boldsymbol{\lambda}_0$ to $\boldsymbol{\lambda}_1$ in the shortest time interval.

The set of voltage vectors that can be generated by the inverter correspond to the $\boldsymbol{U}$ domain. Using a three-phase two level inverter vectors $(\boldsymbol{u}_0, \ldots, \boldsymbol{u}_7)$ as showcase in Figure 2.1. Such an inverter can ideally generate every voltage vector in the area contained by the hexagon, if averaging over a PWM period.

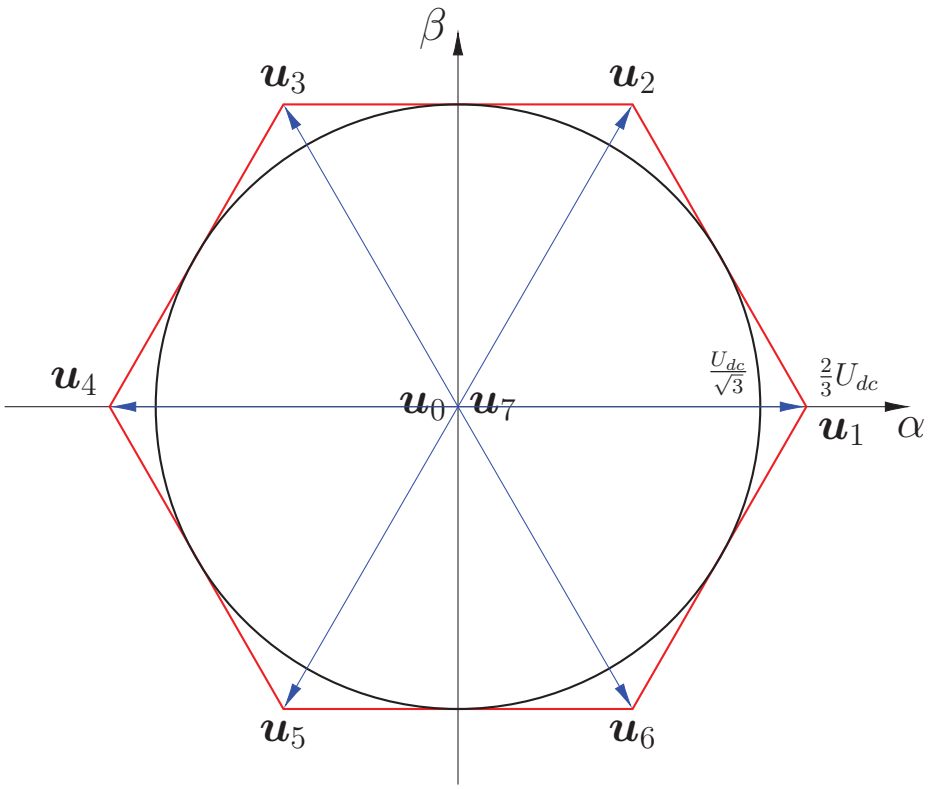

Figure 2.1: Voltage vectors generated by the inverter (the circle shows the voltage amplitude reachable with an non-distorted symmetrical sinusoidal output).

In the following paragraphs, the time optimal problem will be discussed with two different limitations on the $\boldsymbol{U}$ domain: first with a circular one, then with a hexagonal. For what concerns the $\boldsymbol{X}$ domain of flux linkage, the limitation is given by a circle of radius $U_{dc}/(\sqrt{3}|w_{me}|)$, if $\boldsymbol{\lambda}_0$ and $\boldsymbol{\lambda}_1$ are chosen inside said circle, the motor is guaranteed to work in steady state condition.

2.2.1 Circular voltage limit

The optimal control $\bar{\boldsymbol{u}}(t)$ must be searched among the admissible controls with range in $\boldsymbol{U}$. Once a certain admissible control is chosen, for any initial condition $\boldsymbol{\lambda}_0$ the trajectory $\boldsymbol{\lambda} = \boldsymbol{\lambda}(t)$ is uniquely determined by the solution of system (2.14), which is continuos and piecewise differentiable.
Being the system (2.14) linear and under time optimal scenario, the auxiliary system becomes:

$$\dot{\boldsymbol{\psi}} = -\boldsymbol{F}^T \boldsymbol{\psi} \tag{2.16}$$

or explicitly:

$$\begin{bmatrix} \dot{\psi}_1 \\ \dot{\psi}_2 \end{bmatrix} = \begin{bmatrix} 0 & w_{me} \\ -w_{me} & 0 \end{bmatrix} \begin{bmatrix} \psi_1 \\ \psi_2 \end{bmatrix} \tag{2.17}$$

with general solution:

$$\begin{cases} \psi_1 = A\cos(\alpha - w_{me}t) \\ \psi_2 = A\sin(\alpha - w_{me}t) \end{cases} \tag{2.18}$$

where $A > 0$ and α are real scalar constants. For $w_{me} > 0$, $\boldsymbol{\psi}$ describes a clockwise circular trajectory at a constant speed w_{me}. From equation (2.10) the function H becomes:

$$H(\boldsymbol{\psi}, \boldsymbol{\lambda}, \boldsymbol{u}) = w_{me}(\psi_1\lambda_q - \psi_2\lambda_d) + \psi_1 u_d + \psi_2 u_q \tag{2.19}$$

By fixing the values of $\boldsymbol{\psi}$ and $\boldsymbol{\lambda}$, the function $H(\boldsymbol{u})$ describes a plane whose orientation is given by $\boldsymbol{\psi}$. $M(\boldsymbol{\psi}, \boldsymbol{\lambda})$, the upper bound of the function $H(\boldsymbol{u})$ for $\boldsymbol{u} \in \boldsymbol{U}$ is:

$$M(\boldsymbol{\psi}, \boldsymbol{\lambda}) = w_{me}(\psi_1\lambda_q - \psi_2\lambda_d) + A\frac{U_{dc}}{\sqrt{3}} \tag{2.20}$$

and it's reached for $\boldsymbol{u}$ parallel to $\boldsymbol{\psi}$ and belonging to the boundary of the region $\boldsymbol{U}$.
The first condition of the Maximum Principle (which states $H(\boldsymbol{\psi}(t), \boldsymbol{\lambda}(t), \boldsymbol{u}) = M(\boldsymbol{\psi}(t), \boldsymbol{\lambda}(t))\ \forall t | t_0 \leq t \leq t_1$) is easily satisfy by choosing $\boldsymbol{u}(t)$ on the boundary of $\boldsymbol{U}$ and parallel to $\boldsymbol{\psi}(t)$ for all t, $t_0 \leq t \leq t_1$. This implies that the optimal control is a voltage vector belonging to the boundary of $\boldsymbol{U}$ and rotating clockwise at speed w_{me}. This translate to a constant voltage vector in the stationary $\alpha\beta$-frame.

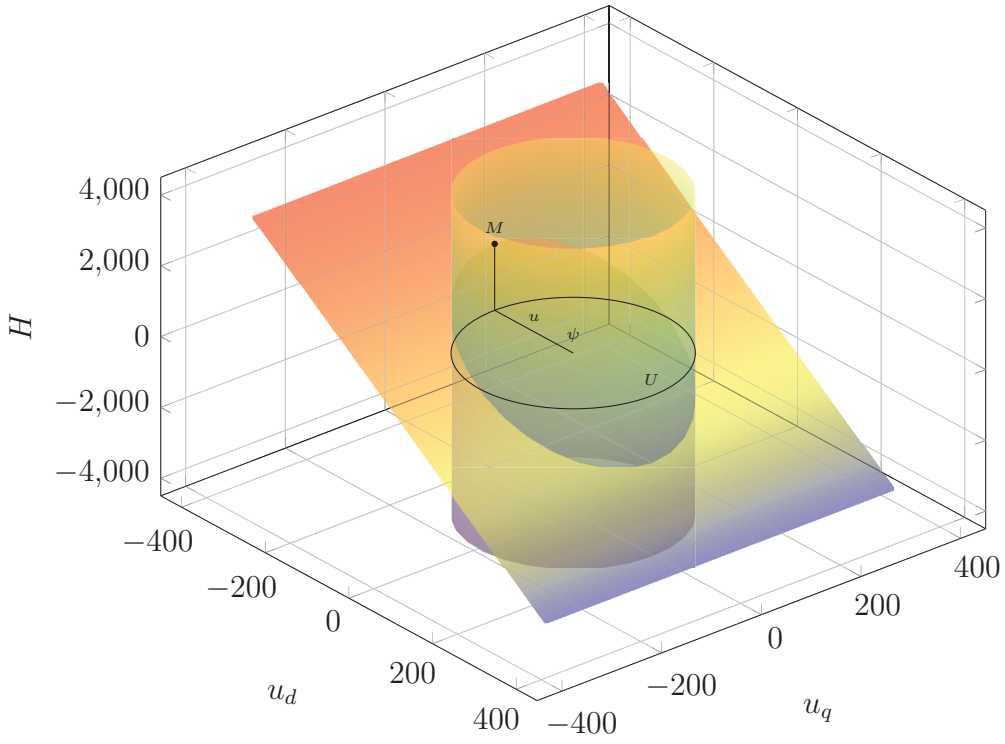

Figure 2.2: Graphical representation of the problem with circular voltage limit.

In figure (2.2) the plane correspond to the function $H(\boldsymbol{u})$ for a given value of $\boldsymbol{\psi}$ and $\boldsymbol{\lambda}$. The circumference is the boundary of domain $\boldsymbol{U}$ and the vector inside it represent vector $\boldsymbol{\psi}$, which also points toward the maximum slope of the plane. It can be easily seen that the maximum of $H(\boldsymbol{u})$ for $\boldsymbol{u} \in \boldsymbol{U}$ is obtained for $\boldsymbol{u}$ belonging to the boundary of $\boldsymbol{U}$ and oriented as $\boldsymbol{\psi}$.
The second condition has also to be verified:

$$M(\boldsymbol{\psi}(t), \boldsymbol{\lambda}(t)) = w_{me}(\psi_1\lambda_q - \psi_2\lambda_d) + A\,\frac{U_{dc}}{\sqrt{3}}\bigg|_{t=t_1} \geq 0$$

substituting equation (2.18) in the previous inequality, yields:

$$w_{me}(\lambda_q(t_1)\cos(\alpha - w_{me}t) - \lambda_d(t_1)\sin(\alpha - w_{me}t)) \geq -A\frac{U_{dc}}{\sqrt{3}}$$

Writing $\lambda_d(t_1)$ and $\lambda_q(t_1)$ of final state $\boldsymbol{\lambda_1}$ as $(\|\boldsymbol{\lambda}_1\|\cos(\angle\boldsymbol{\lambda}_1))$ and $(\|\boldsymbol{\lambda}_1\|\sin(\angle\boldsymbol{\lambda}_1))$ respectively, yields:

$$w_{me}\frac{\sqrt{3}}{U_{dc}}\sin(\angle\boldsymbol{\lambda}_1 - (\alpha - w_{me}t_1)) \geq -1$$

Therefore the inequality is satisfied for $|w_{me}\frac{\sqrt{3}}{U_{dc}}\|\boldsymbol{\lambda}_1\|| \leq 1$ (since sin() belong to the set $[-1, 1]$). Such condition is already part of the hypothesis of the problem. Thus the requirement of the Maximum Principle are satisfied.

Under the above cited hypothesis, a voltage vector belonging to the boundary of a circular control region and constant in the stationary $\alpha\beta$-frame satisfy the necessary conditions required by the Maximum Principle to be time-optimal.

Let's now analyse the problem from the stationary $\alpha\beta$-frame to verify that the result found is really the time optimal one. Operating in such frame, transforms the system (2.14) becomes:

$$\begin{cases} \dfrac{d\lambda_\alpha}{dt} = u_\alpha \\ \dfrac{d\lambda_\beta}{dt} = u_\beta \end{cases} \tag{2.21}$$

and its solution for a generic voltage vector $\boldsymbol{u}_{\alpha\beta}(t)$:

$$\boldsymbol{\lambda}_{\alpha\beta}(t) = \boldsymbol{\lambda}_{\alpha\beta}(0) + \int_0^t \boldsymbol{u}_{\alpha\beta}(\tau)d\tau \tag{2.22}$$

which means that the flux linkage variation in the time interval $[0, t]$ in the stationary $\alpha\beta$-frame is equals to the integral of the voltage applied in the same time interval.
It is clear then that in order to move from a initial point $\boldsymbol{\lambda}_{\alpha\beta}(0)$ in the fastest way possible, the maximum tension vector must be applied during the time interval, and it must be constant to maximise the integral which appears in the solution of (2.21).

2.2.2 Hexagonal voltage limit

In this section it has been replace the circular boundary of $\boldsymbol{U}$ with a hexagonal one, nearer to the real case.
By doing so the problem becomes slightly more difficult, since in the synchronous dq-frame, there will be a hexagon rotating around the centre at $-w_{me}$ speed. To avoid the issue, it is possible to work in the stationary $\alpha\beta$-frame. However, by doing so, the final point, which was stationary in the synchronous frame, now becomes time-variant, as it rotates around the

centre of the frame with w_{me} speed. In such case the first condition of the Maximum Principle holds, while the second one becomes:

$$M(\boldsymbol{\psi}(t_1), \boldsymbol{x}(t_1), t_1) \geq \sum_{\nu=1}^{n} \psi_\nu(t_1) q_\nu \tag{2.23}$$

where

$$(q_1, q_2, \ldots, q_n) = \left.\frac{d\boldsymbol{x}_1}{dt}\right|_{t=t_1} \tag{2.24}$$

Combining equations (2.9) and (2.21), the function H becomes:

$$H(\boldsymbol{\psi}, \boldsymbol{\lambda}, \boldsymbol{u}_{\alpha\beta}) = \psi_1 u_\alpha + \psi_2 u_\beta \tag{2.25}$$

with the vector ψ being constant, as suggests the second equation of the system (2.10). By the considerations made in the circular voltage limit case, a constant voltage vector $\boldsymbol{u}_{\alpha\beta}$ in the stationary frame and belonging to the boundary of control domain is likely to satisfy the time optimality criteria. Since both $\boldsymbol{\psi}$ and $\boldsymbol{u}_{\alpha\beta}$, for a given value of the first, $H(\boldsymbol{u}_{\alpha\beta})$ will draw a time invariant plane. To satisfy the first condition of the Maximum Principle, $\boldsymbol{\psi}$ must be chosen perpendicular to and pointing at the edge of the hexagonal region, where $\boldsymbol{u}_{\alpha\beta}$ lies.

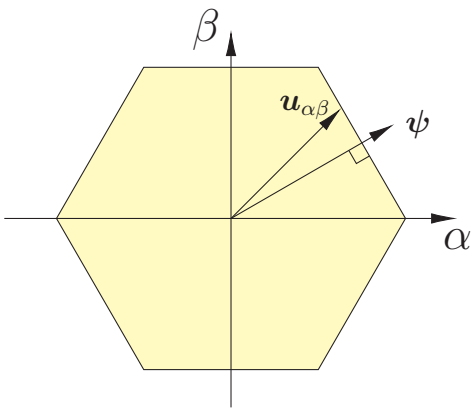

Figure 2.3: Orientation of the co-state $\boldsymbol{\psi}$.

For the second condition it is necessary to rewrite the inequality. As mention before $\boldsymbol{\lambda}_1(t)$ describes a circular trajectory at the w_{me} speed, therefore its derivative respect time is:

$$\begin{cases} q_1 = w_{me} \|\boldsymbol{\lambda}_1\| \cos\alpha \\ q_2 = w_{me} \|\boldsymbol{\lambda}_1\| \sin\alpha \end{cases}$$

vectors $\boldsymbol{\psi}$ and $\boldsymbol{u}_{\alpha\beta}$ can be expressed as:

$$\begin{cases} \psi_1 = \|\boldsymbol{\psi}\| \cos\beta \\ \psi_2 = \|\boldsymbol{\psi}\| \sin\beta \end{cases}$$

$$\begin{cases} u_\alpha = \|\boldsymbol{u}_{\alpha\beta}\| \cos\gamma \\ u_\beta = \|\boldsymbol{u}_{\alpha\beta}\| \sin\gamma \end{cases}$$

therefore inequality (2.23) can be written as:

$$\|\boldsymbol{\psi}\|\|\boldsymbol{u}_{\alpha\beta}\|(\cos\gamma\cos\beta + \sin\gamma\sin\beta) \geq w_{me}\|\boldsymbol{\psi}\|\|\boldsymbol{\lambda}_1\|(\cos\alpha\cos\beta + \sin\alpha\sin\beta)$$

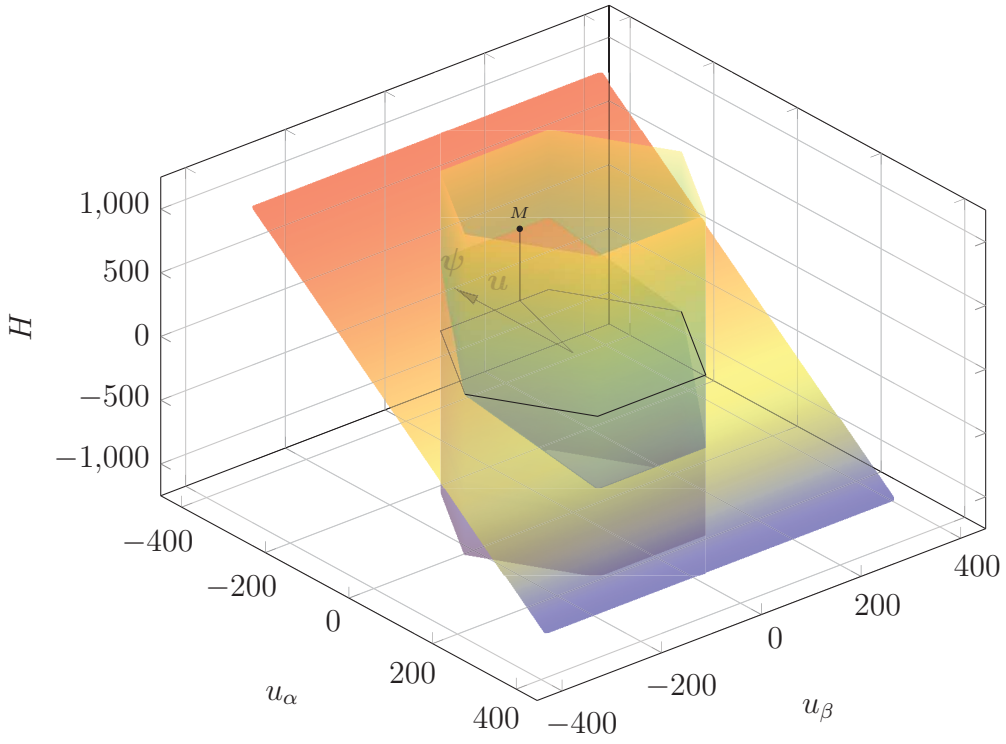

Figure 2.4: Graphical representation of the problem with an hexagonal voltage limit.

which has to be verified. After simplification, the inequality becomes:

$$\|\boldsymbol{u}_{\alpha\beta}\| \cos(\beta - \gamma) \geq w_{me}\|\boldsymbol{\lambda}_1\| \cos(\alpha - \beta)$$

The inequality written above is verified since its left hand side has minimum value equal to $U_{dc}/\sqrt{3}$, in fact the vectors $\boldsymbol{\psi}$ and $\boldsymbol{u}_{\alpha\beta}$ must be on the same

edge and the angle $(\beta-\gamma)$ between the two has value in the interval $\left[-\frac{\pi}{6}, \frac{\pi}{6}\right]$, while for hypothesis $\|\boldsymbol{\lambda}_1\| \leq U_{dc}/\sqrt{3}|w_{me}|$ and $\cos(\alpha-\beta) \leq 1$. Therefore:

> **A voltage vector belonging to the boundary of a hexagonal control region and constant in the stationary $\alpha\beta$-frame satisfies the necessary conditions required by the Maximum Principle to be time-optimal.**

Equation (2.22) still holds and can be rewritten as:

$$\Delta\boldsymbol{\lambda}_{\alpha\beta}(t) = \boldsymbol{\lambda}_{\alpha\beta}(t) - \boldsymbol{\lambda}_{\alpha\beta}(0) = \int_0^t \boldsymbol{u}_{\alpha\beta}(\tau)d\tau \tag{2.26}$$

If a constant voltage vector is applied in the time interval $[0, t]$ then:

$$\Delta\boldsymbol{\lambda}_{\alpha\beta}(t) = \boldsymbol{u}_{\alpha\beta} \cdot t \tag{2.27}$$

so applying all constant voltage vectors on the boundary of the hexagonal region at the time t_1, then $\Delta\boldsymbol{\lambda}_{\alpha\beta}(t_1)$ will also have an hexagonal shape.

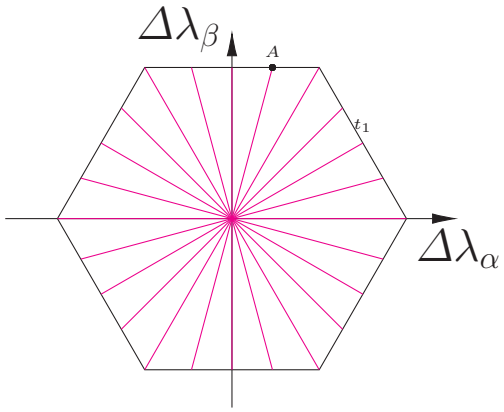

Figure 2.5: Flux linkage variation in a time invariant t_1 in the stationary frame with all constant voltage vectors on the hexagonal voltage limit.

Let's consider now an arbitrary point on the hexagon's boundary of figure 2.5. Said point can also be reached in the same amount of time t_1, using a time-variable control vector $\boldsymbol{u}_{\alpha\beta}(t)$, provided it has the same average over the same time interval of the correspondent constant vector, with exclusion of the vertex, which can only be reached by in t_1 by applying a constant vector $\boldsymbol{u}_{\alpha\beta}$.

Let's assume the desire to reach point A in figure 2.5 using a time variant vector. The β-component of such control can be the same of the constant one only if it belong to the top edge of the hexagonal control region $\boldsymbol{U}$ since it limits the control vector. A right choice of the α-component makes possible to obtain the same α-component as the constant control. The reasoning is analogue with all reachability set's edges. Thus it is not possible to change the flux linkage in a fastest way than by applying a constant voltage vector in the stationary frame. Therefore it is the optimal control.
So it is possible to say:

> **Let $\bar{\boldsymbol{u}}_{\alpha\beta}$ be the optimal constant control which moves the state of the system from $\boldsymbol{\lambda}_0$ to $\boldsymbol{\lambda}_1$ in the time interval $[0, t_1]$, with a hexagonal voltage limit $\boldsymbol{U}$. Any other time-variant voltage vector $\boldsymbol{u}_{\alpha\beta}(t)$ which satisfies $\bar{\boldsymbol{u}}_{\alpha\beta} = \frac{1}{t_1}\int_0^{t_1} \boldsymbol{u}_{\alpha\beta}(t)dt$ is also time-optimal.**
> **Moreover, it turns out that $\bar{\boldsymbol{u}}_{\alpha\beta}$ and $\boldsymbol{u}_{\alpha\beta}$ belong to the same edge of the hexagon.**

2.3 Finding the Optimal Control

In the previous section it has been found the optimal control's features, but not a way to compute it. It is already known that the optimal control consist in a constant vector belonging to the boundary of $\boldsymbol{U}$ in the stationary frame, what it's not known is it's phase. The problem is the following:

> **Given the initial state $\boldsymbol{\lambda}_0$ and the desired state $\boldsymbol{\lambda}_1$, find the phase of the optimal voltage vector $\bar{\boldsymbol{u}}_{\alpha\beta}$ which move the state of the system from $\boldsymbol{\lambda}_0$ to $\boldsymbol{\lambda}_1$ in the shortest time interval.**

If working in the synchronous frame, some other parameters are necessary, such as the ones of the motor, the rotor speed and its position. Porting equation (2.22) to the dq-frame yields the following result:

$$\boldsymbol{\lambda}_{dq}(t_1) = \boldsymbol{\lambda}_{dq}(0)e^{-jw_{me}t_1} + Ue^{j\vartheta_{\alpha\beta}}t_1 e^{-j(\vartheta_{me0}+w_{me}t_1)} \tag{2.28}$$

where $\boldsymbol{\lambda}_{dq}(t_1)$ and $\boldsymbol{\lambda}_{dq}(0)$ are respectively the desired and initial state, w_{me} is the rotor speed, assumed constant during the transient, ϑ_{me0} is the electromechanical position of the rotor at $t = 0$, U and $\vartheta_{\alpha\beta}$ represent the amplitude and phase of the optimal voltage vector. The function U in particular

changes with the type of limitation on the voltage. In case of circular boundary it becomes:

$$U(U_{dc}) = \frac{U_{dc}}{\sqrt{3}} \tag{2.29}$$

while in the hexagonal case:

$$U(U_{dc}, \vartheta_{\alpha\beta}) = \frac{U_{dc}}{\sqrt{3}\sin\left\{\frac{2}{3}\pi - \left[|\vartheta_{\alpha\beta}| - \frac{\pi}{3} fix\left(\frac{3|\vartheta_{\alpha\beta}|}{\pi}\right)\right]\right\}} \tag{2.30}$$

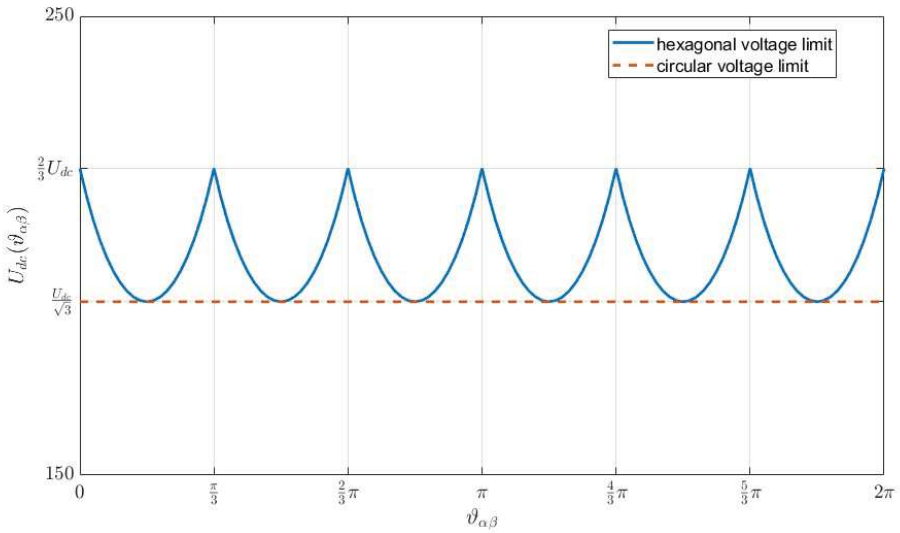

Figure 2.6: Voltage limit as a function of $\vartheta_{\alpha\beta}$.

Combination of equation (2.28) and the appropriate expression for $U_{dc}(\vartheta_{\alpha\beta})$ make up two systems of equations with two unknown: the phase of the voltage vector $\vartheta_{\alpha\beta}$ and the transient time t_1. Finding the transient time means to identify the situation in which the target point belongs to the reachability set, which represent the possible points reachable in a time t_1 from the initial point, and it is indicated with the expression $\mathcal{R}(\lambda_{dq}(0), t_1)$. Finding the phase of the voltage vector means to identify the specific trajectory passing across the target point. The values of these two unknowns will be calculated numerically.
Looking at equation (2.28) it is observable that Ut_1 is equal to the difference between the desired flux $\boldsymbol{\lambda}_{dq}$ and the free response of the initial point $\boldsymbol{\lambda}_{dqc} = \boldsymbol{\lambda}_{dq0} e^{-jw_m e t_1}$:

$$Ut_1 = \sqrt{(\lambda_{d1} - \lambda_{dc}(t_1))^2 + (\lambda_{q1} - \lambda_{qc}(t_1))^2} \tag{2.31}$$

where

$$\begin{cases} \lambda_{dc}(t_1) = \lambda_{d0}\cos(w_{me}t_1) + \lambda_{q0}\sin(w_{me}t_1) \\ \lambda_{qc}(t_1) = -\lambda_{d0}\sin(w_{me}t_1) + \lambda_{q0}\cos(w_{me}t_1) \end{cases} \tag{2.32}$$

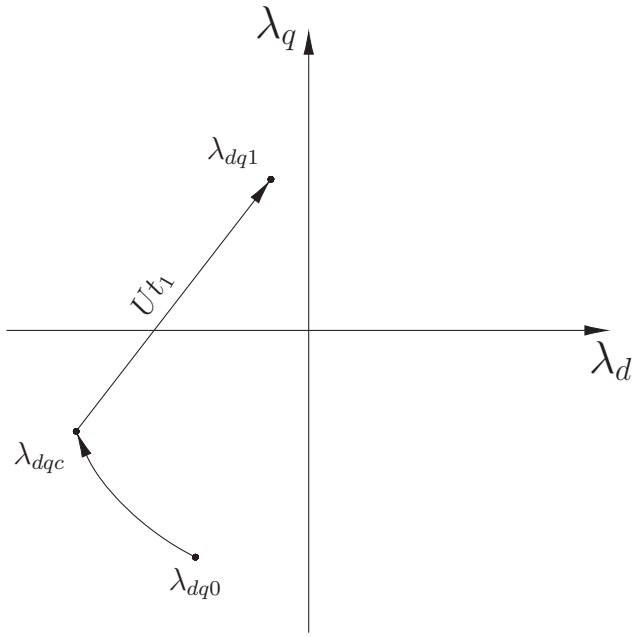

Figure 2.7: Graphical representation of equation 2.31.

In the circular case, the unknown t_1 will be calculated through the bisection method. Once t_1 is known the angle $\vartheta_{\alpha\beta}$ can be calculated by means of the equation:

$$\vartheta_{\alpha\beta} = \angle(\boldsymbol{\lambda}_{dq1} - \boldsymbol{\lambda}_{dqc}) + \vartheta_{me0} + w_{me}t_1 \tag{2.33}$$

With the hexagonal voltage limit, the problem is more complex, a solution will be presented in a future paragraph.

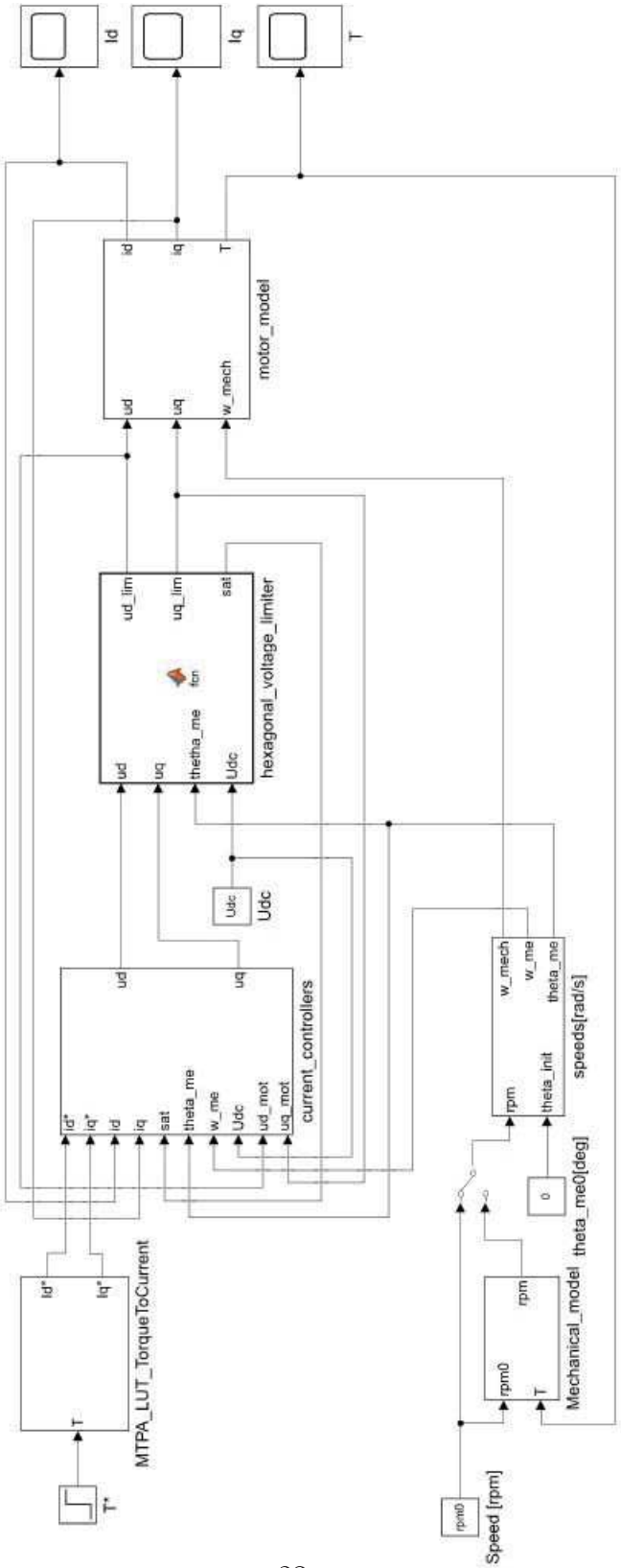

Figure 2.8: SIMULINK® model used for simulations.

Chapter 3

SIMULINK® IPMSM control implementation

In this section it will be presented the control implemented via Matlab® and SIMULINK® to test the time optimal control strategy. Figure 2.8 present the complete scheme of the system. In the next paragraphs each block will be addressed.

3.1 Motor Model

The first block analysed is the motor model. Starting from equations (1.1) and (1.3) it is possible to realize the block that simulates the motor behaviour. Applying the Fourier transform to the state and torque equations, yields:

$$\begin{cases} U_d(s) = RI_d(s) + sL_dI_d(s) - w_{me}L_qI_q(s) \\ U_q(s) = RI_q(s) + sL_qI_q(s) + w_{me}(L_dI_d(s) + \Lambda_m) \\ T(s) = \dfrac{3}{2}pI_q(s)\left[(L_q - L_d)I_d + \Lambda_m\right] \end{cases}$$

The added flux linkage can be eliminated by applying a simple decoupling strategy, which consist in subtracting and adding the flux along the block-scheme. Defining the transfer function of the motor as $H(s) = I(s)/U(s)$ it is obtained:

$$H_d(s) = \frac{1}{R + sL_d}$$

$$H_q(s) = \frac{1}{R + sL_q}$$

The motor scheme becomes the following:

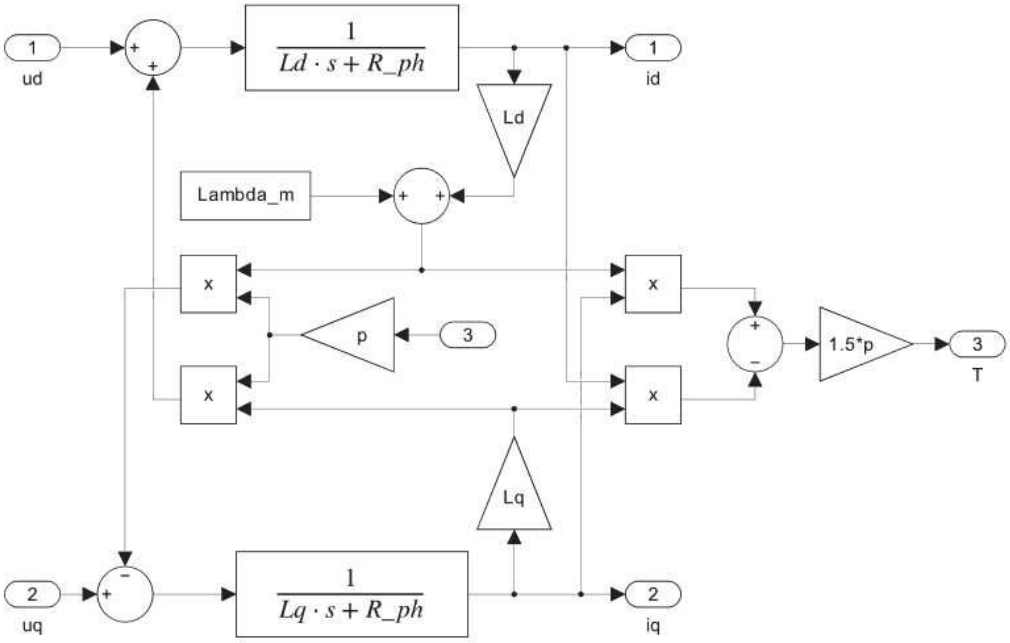

Figure 3.1: SIMULINK® model of the IPMSM.

The model computes current values from the input voltage given to the motor together with the torque, which will be useful to the computation of the rotor position. In this scheme it is also present the first part of the dq-axes decoupling mentioned above, as the fluxes are subtracted from the input voltage.

3.2 Mechanical Model and Speed Block

The objective of these two blocks is to generate the speed and rotor position starting from two possible sources: the speed block, in fact, can compute the electromechanical speed w_{me} and rotor position, starting from a constant value of speed (which impose the condition of constant speed during the transient) or from the output of a mechanical model (in which case the speed is no more constant). This last block in particular computes the mechanical speed w from the torque value generated by the motor model, through the transfer function:

$$M(s) = \frac{1}{B + Js} \tag{3.1}$$

where B is the friction and J is the inertia of the load. In the scheme presented in figure (2.8) two blocks are present, both of which generate a constant

signal, that can be set manually. The first one is the mechanical speed value (in rpm) of the motor which can be selected through a manual switch if a constant speed is to be imposed, otherwise it functions as a value of initial rotor speed, if the mechanical model is selected. The second constant value is the initial rotor position, which sums with the one computed by deriving the electromechanical speed.

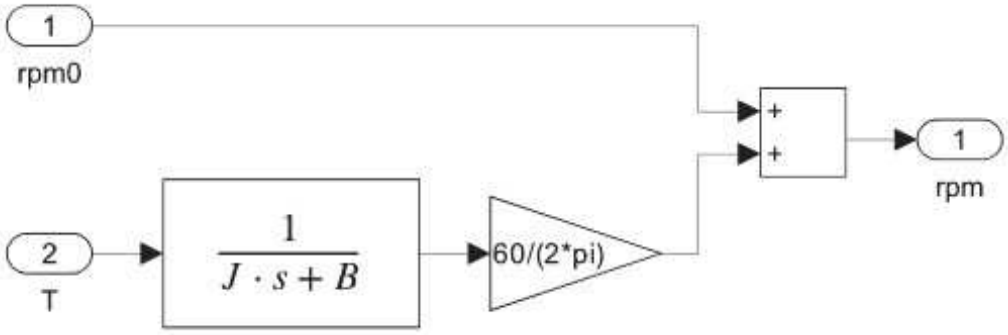

Figure 3.2: SIMULINK® scheme of the Mechanical Model.

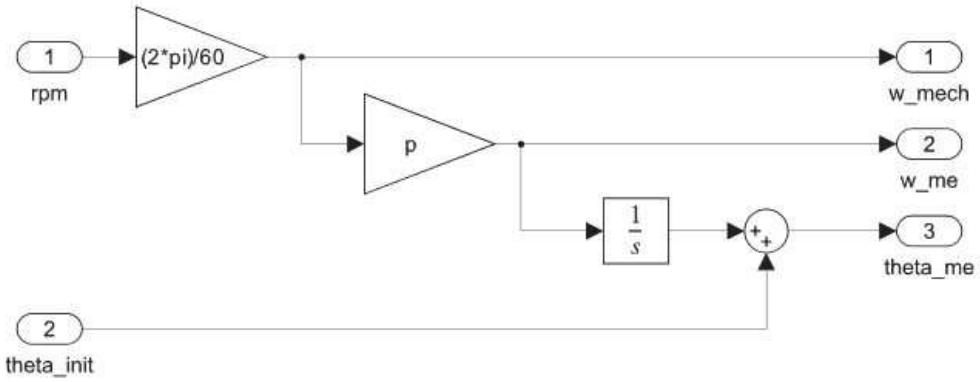

Figure 3.3: Speed and rotor position computation.

3.3 Voltage limiter Block

The Voltage limiter block simulates the average voltage, in a PWM period, that an inverter can output in order to supply a motor. Such block confronts the voltage vector generated by the current controllers block with the

hexagonal voltage limit of the inverter, if the input vector exceeds the limitation than it is shrunk to match the voltage limit, maintaining its phase. The code implementing the function is the following:

```
1   function[ud_lim, uq_lim, sat] = fcn(ud, uq, thetha_me, Udc)
2
3   %alpha,beta voltage coordinates, module and phase computation
4   u_ab_phase = thetha_me + atan2(uq,ud);
5   ua = ud*cos(u_ab_phase) - uq*sin(u_ab_phase);
6   ub = ud*sin(u_ab_phase) + uq*cos(u_ab_phase);
7   U = sqrt(ua^2+ub^2);
8   Uph = atan2(ub,ua);
9
10  U_lim = Udc*sqrt(2/3)/sin(2/3*pi - (abs(Uph) - pi/3*fix(3*abs(Uph)
        /pi))); %Voltage limit angle at angle Uph
11
12  if U_lim < U
13    ua = U_lim*cos(Uph);
14    ub = U_lim*sin(Uph);
15    ud_lim = ub*sin(u_ab_phase) + ua*cos(u_ab_phase);
16    uq_lim = ub*cos(u_ab_phase) - ua*sin(u_ab_phase);
17    sat = 1; %anti-windup enabled (voltage saturated)
18  else
19    ud_lim = ud;
20    uq_lim = uq;
21    sat=0;
22  end
```

in lines 17 and 21 it is also set a flag called "sat" which signals that the voltage saturated. Such flag enables the anti-wind-up system implemented inside the PI current control.

3.4 Current Controllers Block

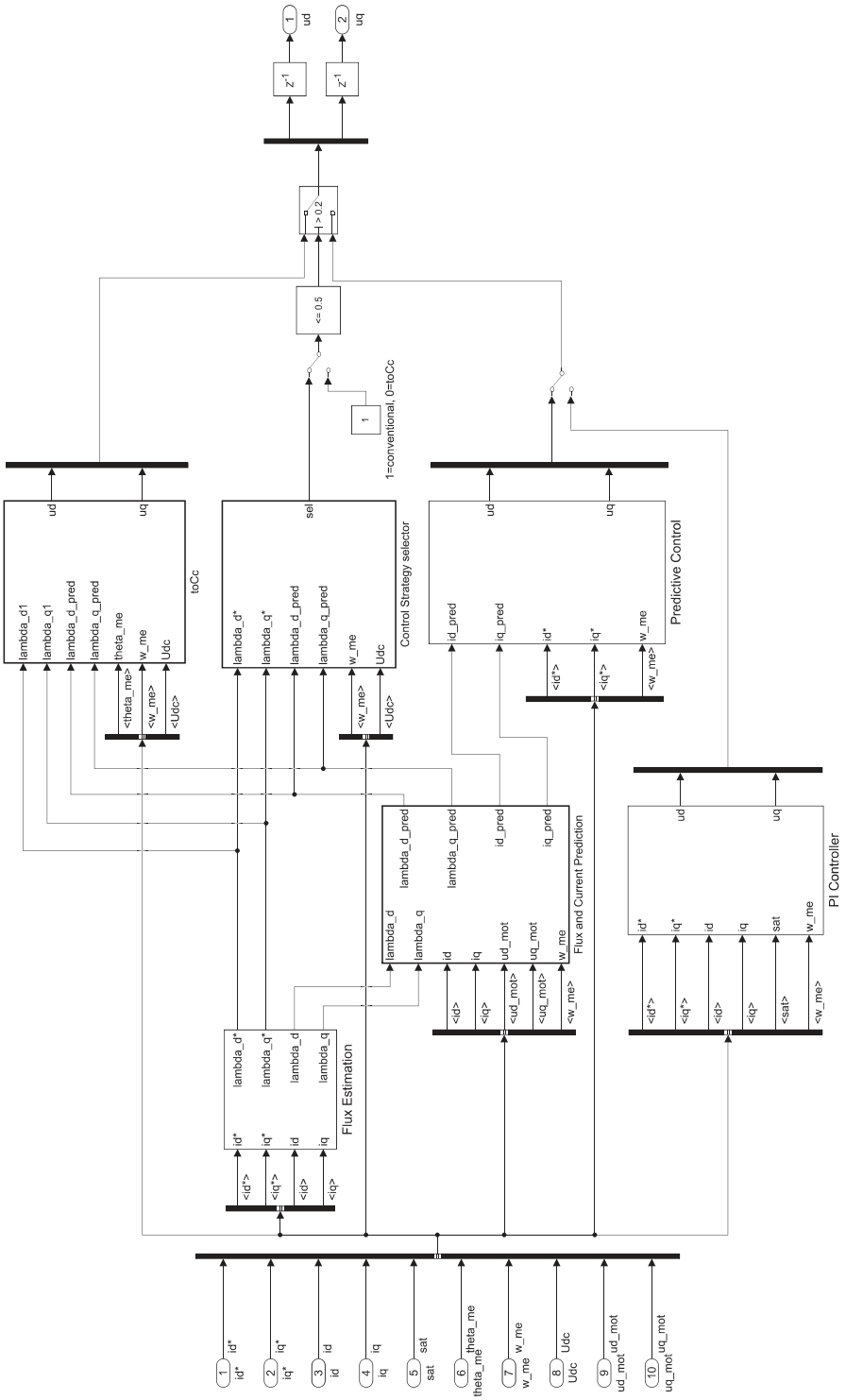

Figure 3.4: Current Controllers scheme.

The scheme, shown in figure (3.4), reports the structure of the `Current_Controllers` Block. In this scheme there are 3 different control strategies implemented: a PI control, a Predictive Control (which shows better performances than the PI and helps the *toCc*) and the *toCc*, whom theory has been studied in the previous chapter.

3.4.1 PI Control

A traditional PI control was firstly modelled, which will serve as a comparison base to study the *toCc* strategy qualities.
The transfer function of the uncontrolled motor along d- and q-axis is:

$$T(s) = \frac{1}{R + sL} \cdot \frac{k_c}{1 + sT_s}$$

where L takes value L_d or L_q, depending on the axis took into consideration, T_s is the period of the PWM generated by the inverter (which coincide with the sampling time of the system) at $100\mu s$ ($f_s = 10kHz$) and k_c is the inverter voltage gain, which it has been set at 1 for simplicity.
Starting from the function above it is possible to model the control, whose formula is:

$$P(s) = k_{i_i} \frac{1 + sT_{PI_i}}{s}$$

where $T_{PI} = k_{p_i}/k_{i_i}$ and k_{p_i} and k_{i_i} are respectively the proportional and integrative constants of the PI control. Placing the crossing frequency at $w_{c_i} \cong 3770rad/s (\cong 600Hz)$ and $T_{PI_i} = L/R$ for simplicity, it is possible to calculate the value of k_{i_i}, by imposing $\|W(jw_{c_i})\| = \|P(jw_{c_i})T(jw_{c_i})\| = 1$:

$$k_{i_i} = \frac{R}{k_c} w_{c_i} \sqrt{1 + (w_{c_i} T_s)^2} \tag{3.2}$$

once found the value of k_{i_i} it is possible to calculate k_{p_i}, since $T_{PI_i} = k_{p_i} k_{i_i}$.
Therefore the values obtained are:

- $k_{i,i_d} = k_{i,i_q} = 1,837e4$
- $k_{p,i_d} = 113.3$
- $k_{p,i_q} = 577.83$

and the bode diagram of the open loop frequency response $W(jw)$ is:

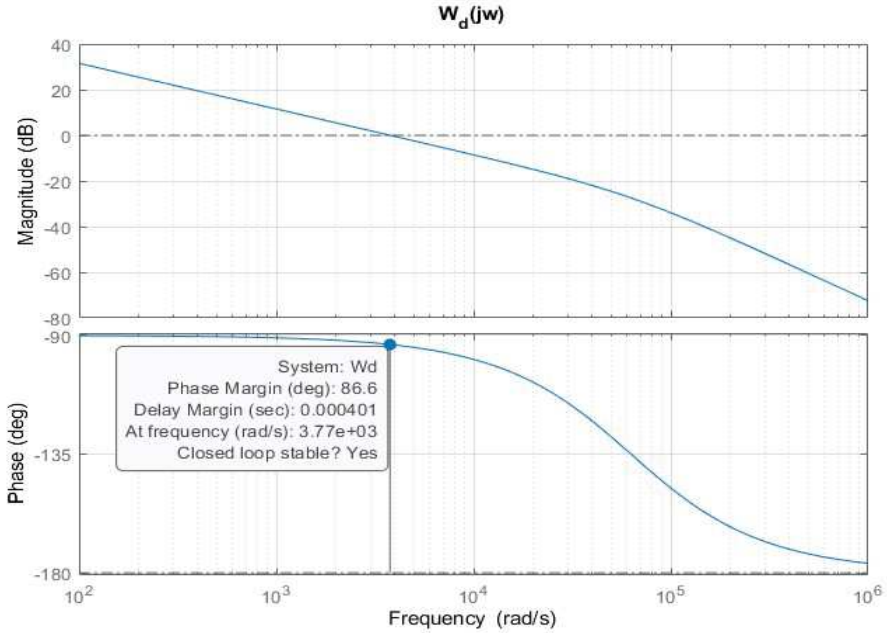

Figure 3.5: Bode diagram of the open loop control along d-axis.

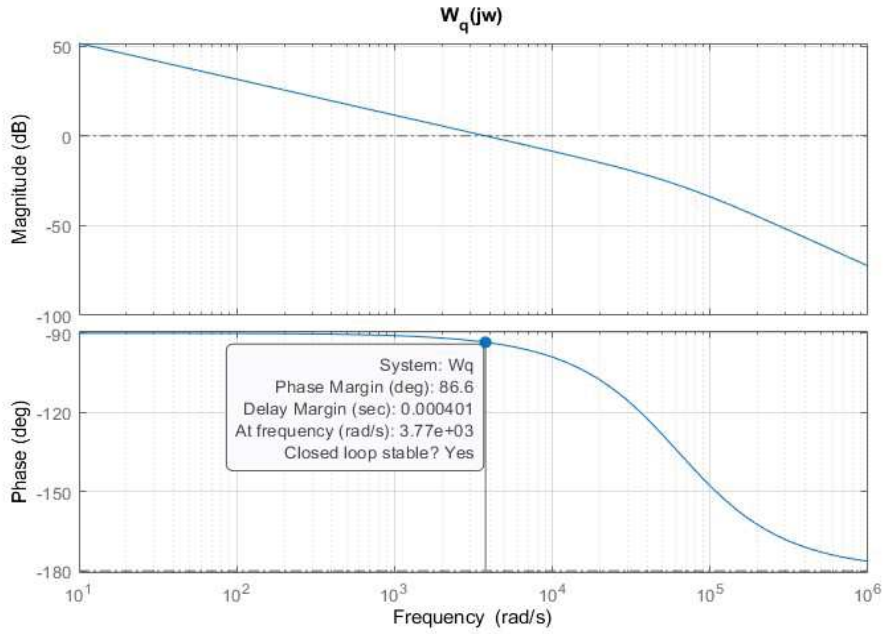

Figure 3.6: Bode diagram of the open loop control along q-axis.

as reported in the bode diagrams above, in both axis the phase margin is $\phi_m = 86.6°$ and the crossing happens at a $-20dB/dec$ slope, therefore the system is stable at close loop, for the *Bode Theorem*. The control produces the following transient:

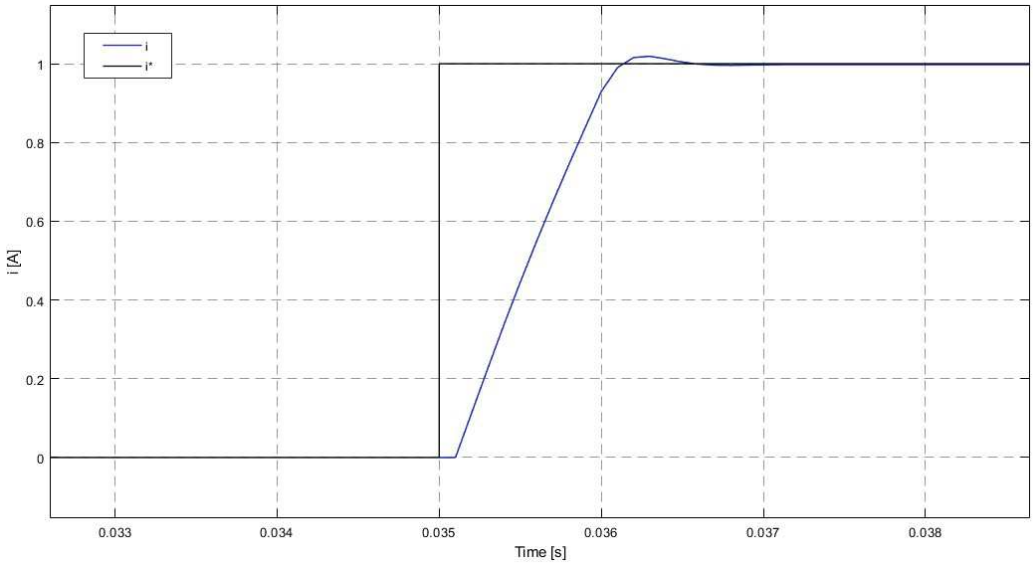

Figure 3.7: Current transient form 0 to 1 A.

To further improve the PI control is also possible to add an anti-wind-up system which disengages the integrative part of the control in case of voltage saturation, provided that the voltage reference u_d^*/u_q^* and the current error of the respective axis would have the same sign. Figure shows the improvement in the transient overshot.

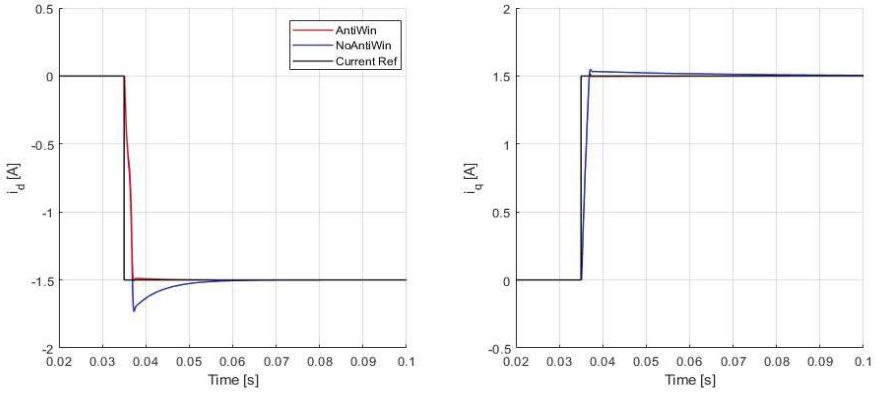

Figure 3.8: Anti-windup performance.

However, if a bigger transient is applied the current step response becomes atypical, an example can be seen in figure (3.9).

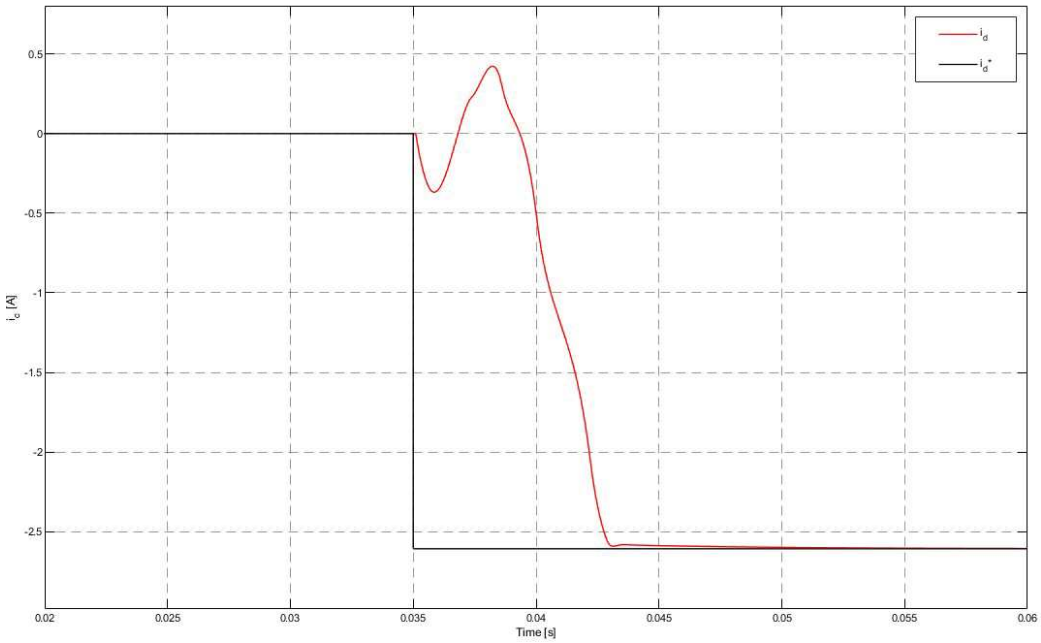

Figure 3.9: i_d current transient with $U_{dc} = 230\ V_{eff}$ $(0 \rightarrow T_n, n_0 = 1500\ rpm)$.

Such anomaly in the transient is due to the low value of the U_dc bus voltage applied to the motor. If a great step is requested to the motor (for example from 0 to the nominal torque value) only a low current can be injected in the motor, thus deforming the transient as shown in figure (3.9).

To improve the plot, the bus voltage could be increased to raise the available power. Imposing a bus voltage $U_{dc} = 380\ V_{peak}$ yields the following result:

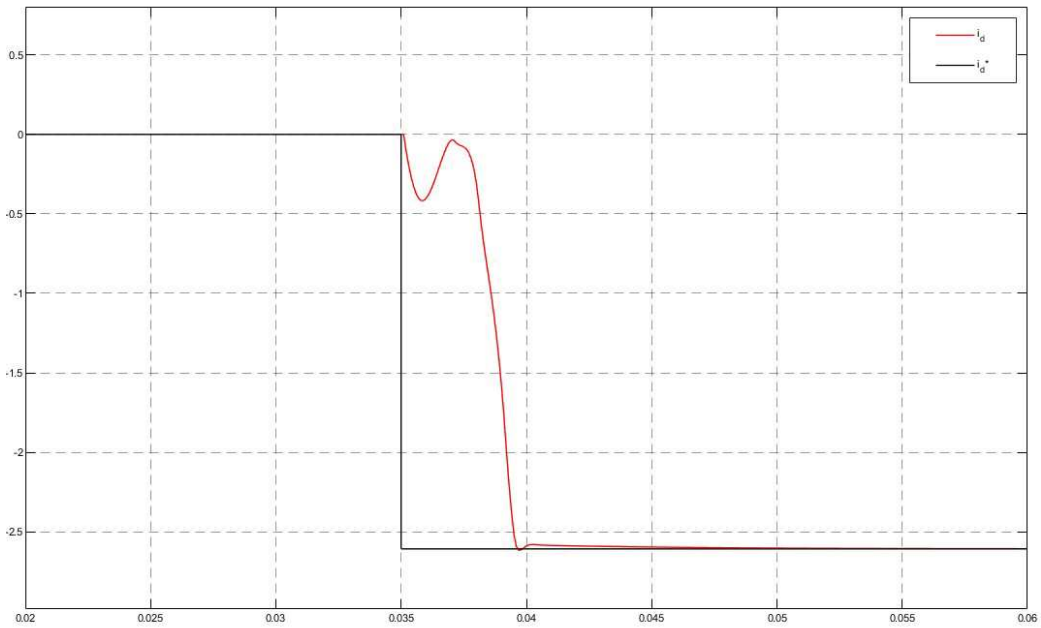

Figure 3.10: i_d current transient with $U_{dc} = 380\ V_{peak}$ $(0 \rightarrow T_n, n_0 = 1500\ rpm)$.

It is clear by looking at figures 3.9 and 3.10 that the second one is better, even if still not completely regular.

The scheme of the PI controller at the end becomes:

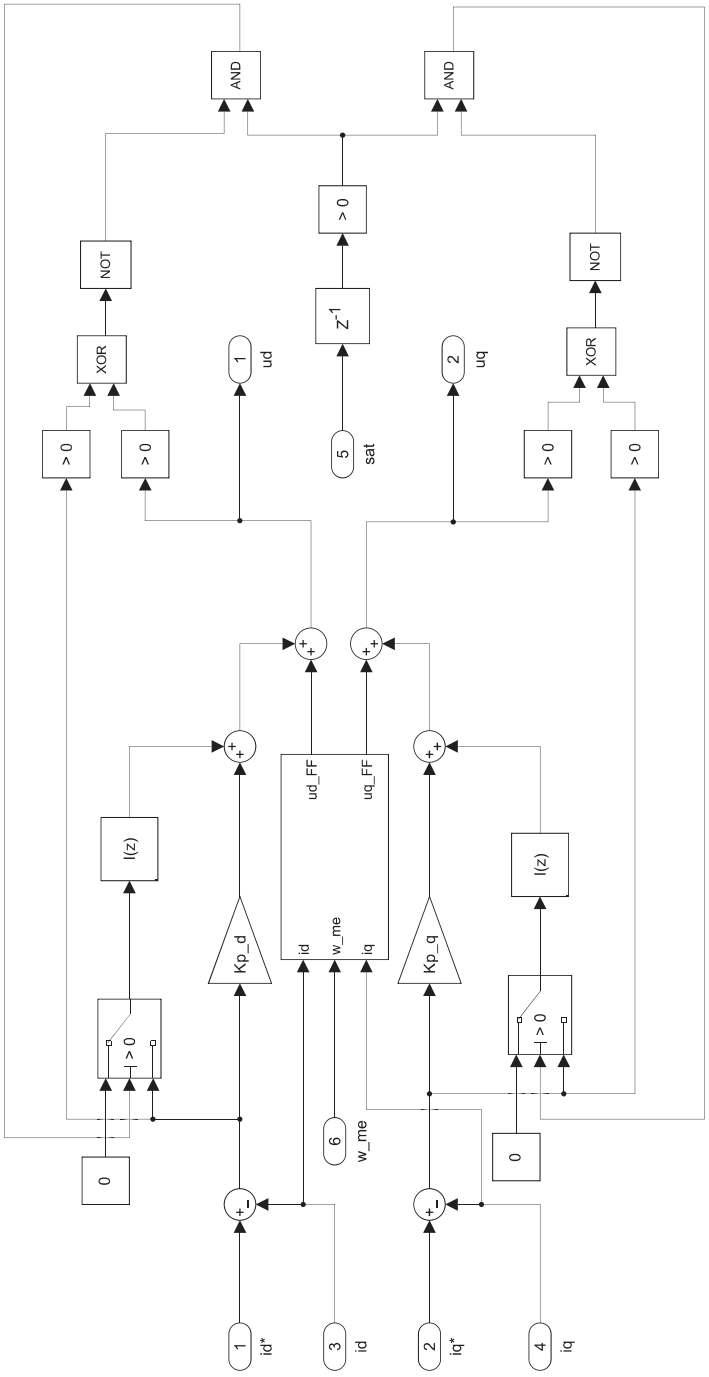

Figure 3.11: PI controller block view, in blue is marked the anti-wind-up scheme.

3.4.2 Control strategy selector

Pivotal to the correct functioning of the control is the `Control Strategy selector`. The *toCc* algorithm, in fact, performs badly in steady state region, as shown in figure 3.12.

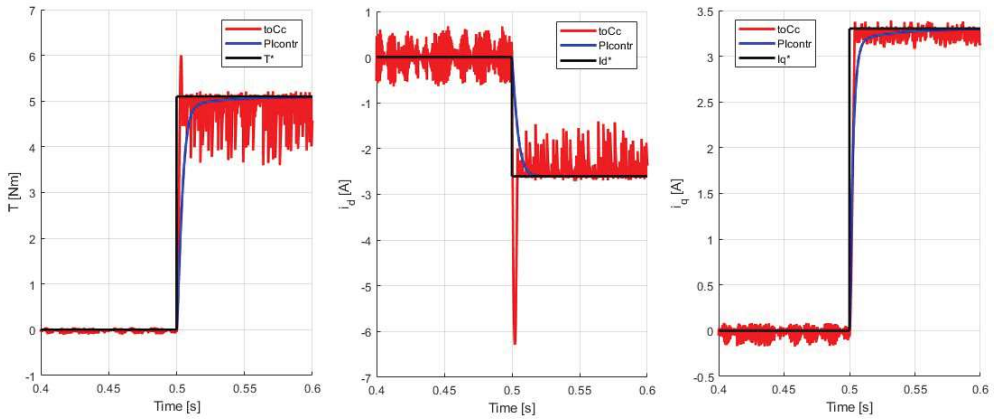

Figure 3.12: Torque and current chattering.

Looking at the pictures of the figure above it is clear the presence of a great ripple in steady state which can arrive up to the 30% of their respective rated value, which is not tolerable.
With such behaviour it becomes necessary to create a control strategy, which can select the most suitable control for each working conditions that arise. The overall performance of the current control strongly depends on the performance of the current control selector. Unnecessary *toCc* actions have to be avoided and a smooth and neat transition between the two control strategies has to be guaranteed.
To carry out such tusk, a flux linkage error amplitude method was proposed. Let us suppose that the motor current i_{dq} is controlled by the conventional current regulator. As long as the current reference i^*_{dq} belongs to the reachability set $\mathcal{R}_{\mathbf{U}}(i_{dq}, T_s)$, where T_s is the sampling time, the current control should be able to track the current reference with a small current error. As soon as the current reference leaves the reachability set, the available voltage is no longer enough to track the reference point, which means that the current would be better controlled by the *toCc*. After the commutation from the conventional control to the *toCc*, the latter must keep working as long as the current reference doesn't belong to the reachability set. To simplify the problem it will be used a circular shaped reachability set.

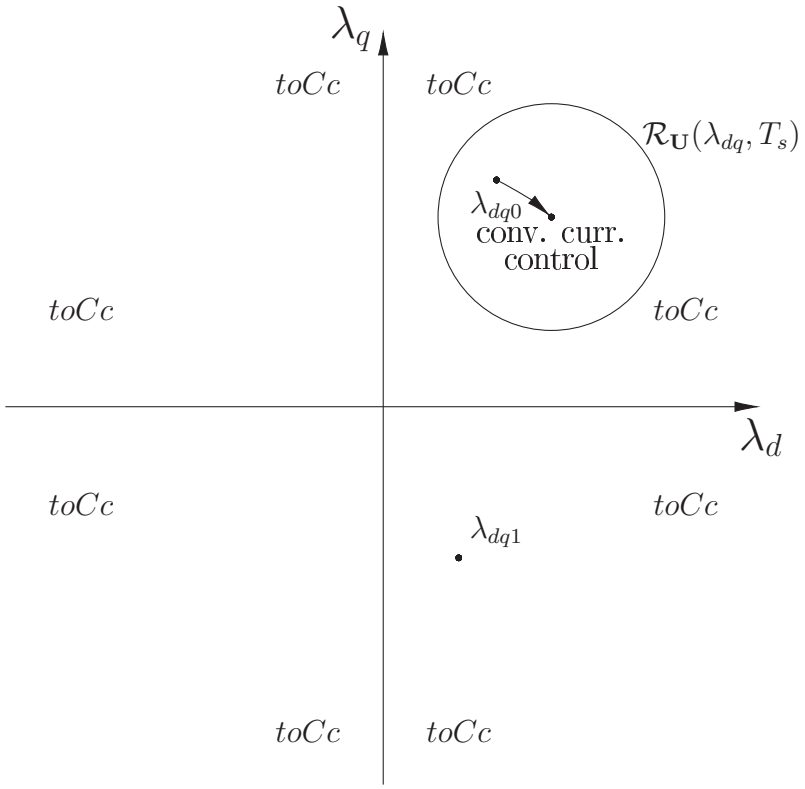

Figure 3.13: $(toCc)$/(conventional current control) selection.

The selection block in the scheme of figure 3.4 works in a slightly different way, but it yields the same result. Instead of using the reachability set $\mathcal{R}_{\mathbf{U}}(\boldsymbol{\lambda_{dq}}, T_s)$, it uses the controllability set $\mathcal{C}_{\boldsymbol{U}}(\boldsymbol{\lambda_{dq1}}, T_s)$, which is a circular region of radius UT_s and centre $\lambda_{dq1}e^{jw_{me}T_s}$. The output of the $toCc$ is selected when the actual flux linkage doesn't belong to $\mathcal{C}_{\boldsymbol{U}}(\boldsymbol{\lambda_{dq1}}, T_s)$, otherwise the output of the traditional current control is selected. The code implemented is the following:

```
1   function sel = fcn(lambda_d1, lambda_q1, lambda_d_pred,
        lambda_q_pred, w_me, Udc)
2   pos = w_me/10e3;
3   lambda_dC = lambda_d1*cos(pos) - lambda_q1*sin(pos);
4   lambda_qC = lambda_d1*sin(pos) + lambda_q1*cos(pos);
5   max_dist = Udc/sqrt(3/2)/10e3;
6   dist = sqrt((lambda_dC-lambda_d_pred)^2 + (lambda_qC-lambda_q_pred
        )^2);
7   if max_dist > dist
8     sel = 1;
9   else
10    sel = 0;
11  end
```

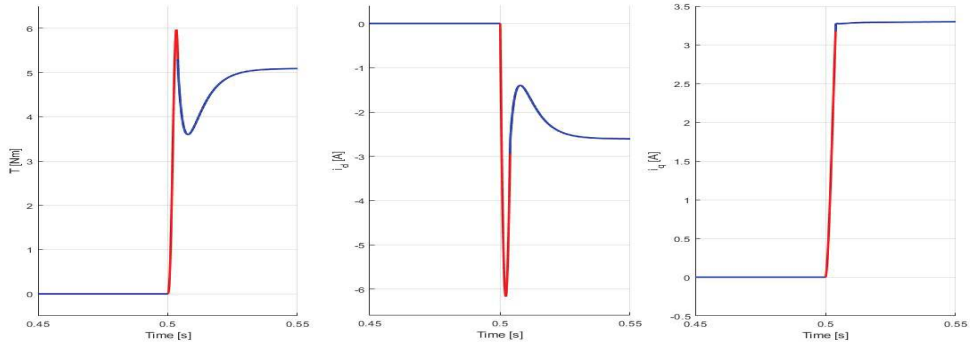

Figure 3.14: Combined action of *toCc* and PI current control (in red is the portion in which the *toCc* operates).

3.4.3 Predictive Control

To simulate the implementation on a digital control platform it has been introduced a delay block at the output of the controllers block. Such a delay unfortunately worsen the selection strategy.

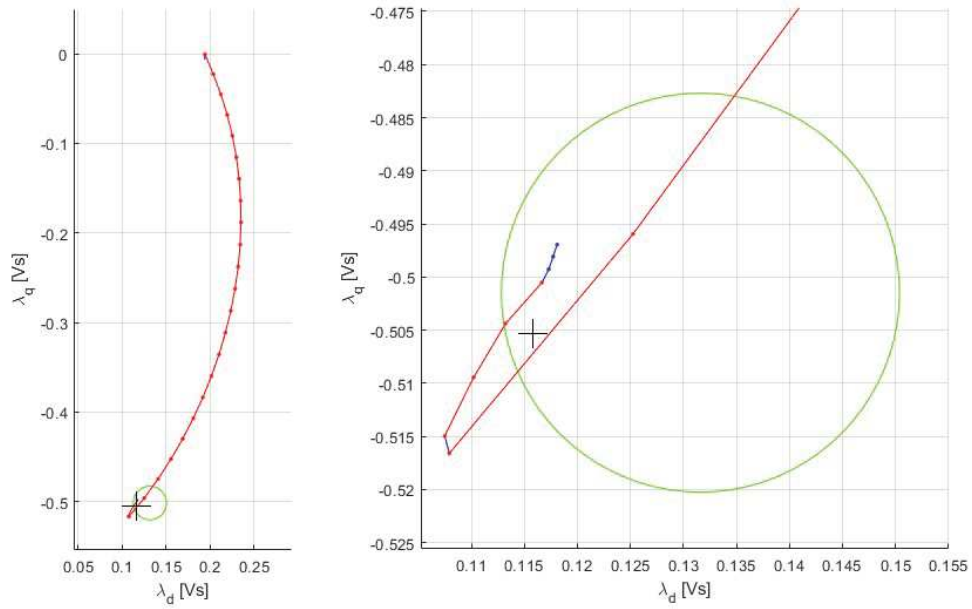

Figure 3.15: "Landing" without current/flux prediction (in red is marked the portion of graph where the *toCc* is active).

In figure 3.15 it is presented the flux linkage in the dq-frame during a transient from 0 to negative rated torque at 1500 rpm, in the second image it is presented a zoomed portion of the graph on the left. The cross represents the target point λ_{dq1}, the circle corresponds to the controllability set of the point λ_{dq1} for a time equal to the sampling time T_s ($100\mu s$). Each dot along the plot correspond to a sample. The state of the system is moved by the *toCc* algorithm toward the controllability set $\mathcal{C}_U(\lambda_{dq1}, T_s)$, but, once reached such region, the control takes an additional step instead of switching to the PI control (additionally the simulation was truncated in order to improve the reliability of the plot).
To compensate for the delay it is necessary to use a predictive control, to replace the original one. Lets consider the generic quantity $x(k)$ where k represent the sample. Lets also indicate with $\bar{x}_k$ the average quantity value between sample k and $k+1$. Figure 3.16 shows a graphical representation of what has been described.

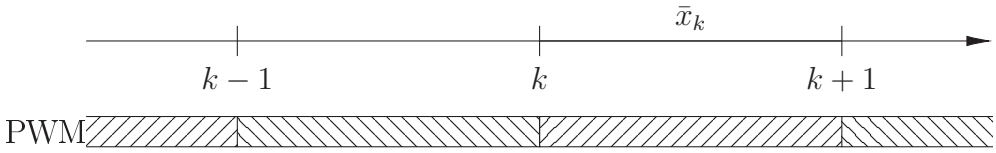

Figure 3.16: Discrete time line.

Using this convention on the system 1.1 becomes:

$$\begin{cases} \bar{u}_{d_k} = \dfrac{\lambda_{d_{k+1}} - \lambda_{d_k}}{T_s} - w_{me}\bar{\lambda}_{q_k} + R\bar{i}_{d_k} \\ \bar{u}_{q_k} = \dfrac{\lambda_{q_{k+1}} + \lambda_{q_k}}{T_s} - w_{me}\bar{\lambda}_{d_k} + R\bar{i}_{q_k} \end{cases} \tag{3.3}$$

where T_s is the sampling time, k is the last acquired sample and $\bar{\boldsymbol{i}}_{dq_k}$ and $\bar{\boldsymbol{\lambda}}_{dq_k}$ are approximated by the expression:

$$\bar{\boldsymbol{i}}_{dq_k} = \frac{\boldsymbol{i}_{dq_{k+1}} + \boldsymbol{i}_{dq_k}}{2} \quad \bar{\boldsymbol{\lambda}}_{dq_k} = \frac{\boldsymbol{\lambda}_{dq_{k+1}} + \boldsymbol{\lambda}_{dq_k}}{2} \tag{3.4}$$

What is needed is to predict the state of the system $\boldsymbol{\lambda}_{dq_{k+1}}$ at sample $k+1$. By substituting $\bar{\boldsymbol{u}}_{dq_k} = \boldsymbol{u}^*_{dq}$ and equations 3.4 into system 3.3 it is obtained:

$$\begin{cases} \lambda_{d_{k+1}} - \dfrac{w_{me}T_s}{2}\lambda_{q_{k+1}} + \dfrac{RT_s}{2}i_{d_{k+1}} = \left(u^*_{d_k} + \dfrac{w_{me}}{2}\lambda_{q_k} - \dfrac{R}{2}i_{d_k}\right)T_s + \lambda_{d_k} \\ \lambda_{q_{k+1}} + \dfrac{w_{me}T_s}{2}\lambda_{d_{k+1}} + \dfrac{RT_s}{2}i_{q_{k+1}} = \left(u^*_{q_k} - \dfrac{w_{me}}{2}\lambda_{d_k} - \dfrac{R}{2}i_{q_k}\right)T_s + \lambda_{q_k} \end{cases} \tag{3.5}$$

An other substitution must be applied on the current, since its value at sample $k+1$ isn't known. The substitution is the following:

$$\begin{cases} i_{d_{k+1}} = \dfrac{\lambda_{d_{k+1}} - \Lambda_{mg}}{L_d} \\ i_{q_{k+1}} = \dfrac{\lambda_{q_{k+1}}}{L_q} \end{cases} \tag{3.6}$$

System 3.5 becomes the following:

$$\begin{cases} a_{11}\lambda_{d_{k+1}} + a_{12}\lambda_{q_{k+1}} = b_1 \\ a_{21}\lambda_{q_{k+1}} + a_{22}\lambda_{q_{k+1}} = b_2 \end{cases} \tag{3.7}$$

where

$$\begin{cases} a_{11} = 1 + \dfrac{RT_s}{2L_d} \\ a_{21} = -\dfrac{w_{me}T_s}{2} \\ a_{21} = -a_{12} \\ a_{22} = 1 + \dfrac{RT_s}{2L_q} \\ b_1 = \left[u^*_{d_k} + \dfrac{w_{me}}{2}\lambda_{q_k} - \dfrac{R}{2}\left(i_{d_k} - \dfrac{\lambda_{mg}}{L_d}\right)\right] T_s + \lambda_{d_k} \\ b_2 = \left(u^*_{q_k} - \dfrac{w_{me}}{2}\lambda_{d_k} - \dfrac{R}{2}i_{q_k}\right) T_s + \lambda_{q_k} \end{cases}$$

It is now possible to calculate the value of $\lambda_{d_{k+1}}$ and $\lambda_{q_{k+1}}$ since system 3.7 is linear, with two equation in two unknown. Once they are found it is also possible to calculate the predicted currents $i_{d_{k+1}}$ and $i_{q_{k+1}}$, by means of flux linkage formula.
Once all the necessary values are known the predictive control calculates the voltage to be applied by means of the system:

$$\begin{cases} u^*_d = Ri_{d_{pred}} + (i^*_d - i_{d_{pred}})\dfrac{L_d}{T_s} - w_{me}L_q i_{q_{pred}} \\ u^*_q = Ri_{q_{pred}} + (i^*_q - i_{q_{pred}})\dfrac{L_q}{T_s} + w_{me}\left(L_d i_{d_{pred}} + \Lambda_{mg}\right) \end{cases} \tag{3.8}$$

which is the system 1.2 written using the Euler method. If the predicted flux linkage is used in the *toCc* algorithm and in the control selection the result is shown in figure (3.17). By comparing it with figure (3.15) it is clear that the landing with the predictive control is neater.

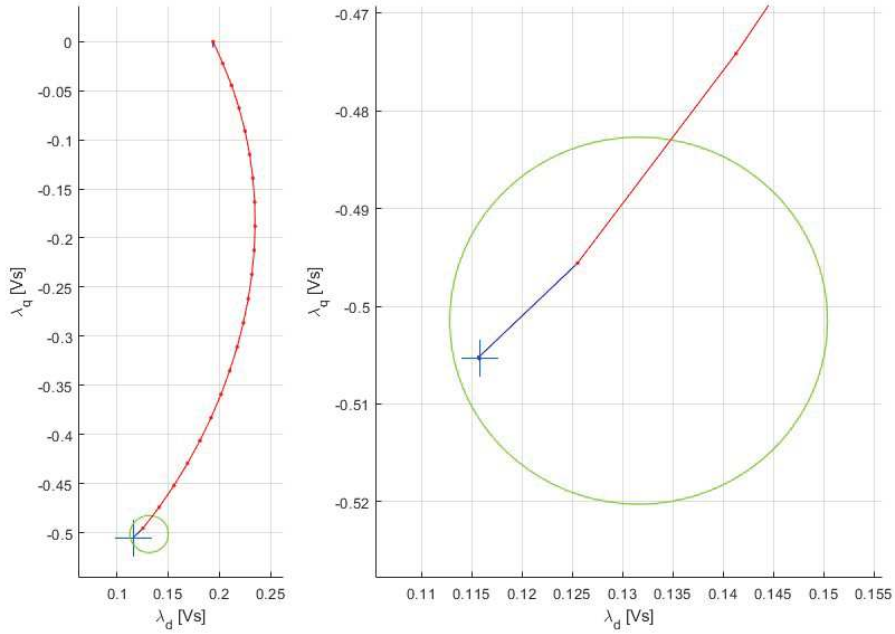

Figure 3.17: "Landing" with current/flux prediction (in red is marked the portion of graph where the *toCc* is active).

3.4.4 Time Optimal Current Control (*toCc*)

Of particular relevance is the block which implements the *toCc*. As aforementioned, the *toCc* algorithm works with the flux linkages. In light of that a `Flux Estimation` block has been implemented which calculates the desired flux linkage and the current one by means of the known relationship between the currents and the flux linkages of the specific motor, which then is used to calculate the predicted one through the Flux and Current Prediction block, as specified in the previous paragraph.
The code which implements the *toCc* strategy is the sequent:

```
1   function [ud, uq] = fcn(lambda_d1, lambda_q1, lambda_d_pred,
        lambda_q_pred, theta_me, w_me, Udc)
2
3     t_min = 0;    % [s]
4     t_max = 15e-3;  % [s]
5     t = 0.5*(t_min+t_max);
6
7     % bisection algorithm
8     for dummy=1:20
9       pos = w_me*t;
10      lambda_dc = lambda_d_pred*cos(pos)+lambda_q_pred*sin(pos);
11      lambda_qc = -lambda_d_pred*sin(pos)+lambda_q_pred*cos(pos);
```

```
12        delta_d = lambda_d1-lambda_dc;
13        delta_q = lambda_q1-lambda_qc;
14        mod = sqrt(delta_d^2+delta_q^2);
15        u_phase_ab = atan2(delta_q, delta_d)+theta_me+pos;
16        Vhex = Udc/sqrt(3/2)/sin(2/3*pi-(abs(u_phase_ab)-pi/3*fix(3*
              abs(u_phase_ab)/pi)));
17        max_mod = Vhex*t;
18        if mod > max_mod
19          t_min = t;
20        else
21          t_max = t;
22        end
23        t = 0.5*(t_min+t_max);
24      end
25
26      % phase of the voltage reference vector in the synchronous dq
            frame
27      u_phase_dq = atan2(delta_q, delta_d)+pos;
28
29      % Amplitude of the voltage reference vector: its amplitude
30      % is shrunk by the voltage limiter block.
31      u_amp = 2/3*Udc*sqrt(2);
32
33      ud = u_amp*cos(u_phase_dq); % d-axis voltage reference [V]
34      uq = u_amp*sin(u_phase_dq); % q-axis voltage reference [V]
```

where `lambda_d1` is λ_{d1}, `lambda_d0` is λ_{d0}, `lambda_dc` is $\lambda_{dc}(t_1)$ and `t` is t_1. Lines 3-4 set the range where the solution of equation (2.31) is sought. The minimum time (`t_min`) is set to zero, and the maximum time (`t_max`) must be greater than the length of the longest possible torque transient. Such value can be calculated by knowing that the longest possible transient corresponds to a diameter of a circle of radius 0.41 Vs (the largest flux linkage transient) and the smallest voltage vector amplitude corresponds to $Udc/\sqrt{(3)} \cong 188\,V$. With these data, the longest transient turns out to be $0.82/188 \cong 4.4\ ms$. Taking a large safety factor, `t_max` can be set at 15 ms.

The bisection method was implemented with a *for* loop. Such loop guarantees a constant and known execution time and does not give rise to possible dangerous infinite loops. After n iterations t_1 is less than $(t_{max}-t_{min})/2n+1$, which is approximately 7 ns for the specific case. Once the transient time `t` is known, the phase of the voltage vector can be computed from equation (2.33).

In the figure below it has been reported the voltage amplitude and phase during the transient from 0 Nm to the rated torque value at 1500 rpm. In red it has been also emphasized the portion in which the *toCc* algorithm is working. Noticeable is the phase of the voltage which remains almost constant, as required by the *toCc*

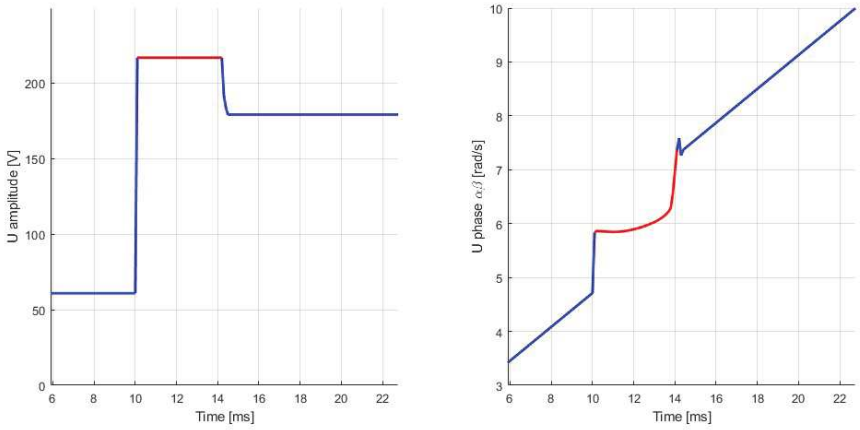

Figure 3.18: Amplitude and phase of voltage during transient.

3.5 Results

In this section will be presented a table where it will be reported the rise time of a number of different transient. It will be also analysed some of the behaviours and drawbacks of this control strategy.
To carry out the simulations the reference current vector was generated via a MTPA (Maximum Torque Per Ampére) lookup table, calculated by using the formula:

$$\gamma = \arccos\left(\frac{-\Lambda_{mg} + \sqrt{\Lambda_{mg}^2 + 8\left(L_d - L_q\right)^2 I^2)}}{4\left(L_d - L_q\right) I}\right)$$

where I is the amplitude of the $\boldsymbol{I}$ current vector in the dq-frame and γ is its phase value necessary for the current vector to lay on the MTPA curve.

3.5.1 Transient Time

Start Point	Target Point	Speed [rpm]	PI rise time [ms]	*toCc* rise time [ms]
0	T_n	750	2.749	2.159
0	T_n	1125	3.627	1.846
0	T_n	1500	6.524	1.614
T_n	0	750	1.392	1.345
T_n	0	1125	1.033	1.016
T_n	0	1500	0.770	0.772
0	$T_n/2$	750	1.765	1.430
0	$T_n/2$	1500	2.487	1.285
$T_n/2$	0	750	1.133	1.124
$T_n/2$	0	1500	0.930	0.901
0	$T_n/5$	750	0.977	0.929
0	$T_n/5$	1500	1.205	0.891
$T_n/5$	0	750	0.677	0.674
$T_n/5$	0	1500	0.601	0.587

Table 3.1: Transient rise time of PI and *toCc* controls.

In the table above it has been presented some possible Torque transients at different rotor speeds. It is clear how the *toCc* algorithm implemented yields the fastest transient. In particular the biggest time saved (equal to $4.910\ ms$) can be seen in the third transient ($T_n \rightarrow -T_n$ at $1500\ rpm$).
An other observation can be made about the variation of the rise time related to speed. As the speed rises, the rise time becomes lower for the *toCc*. The rotor speed explicitly appears in the electric equations of the motor. For this reason, the torque transients are affected by the speed value.

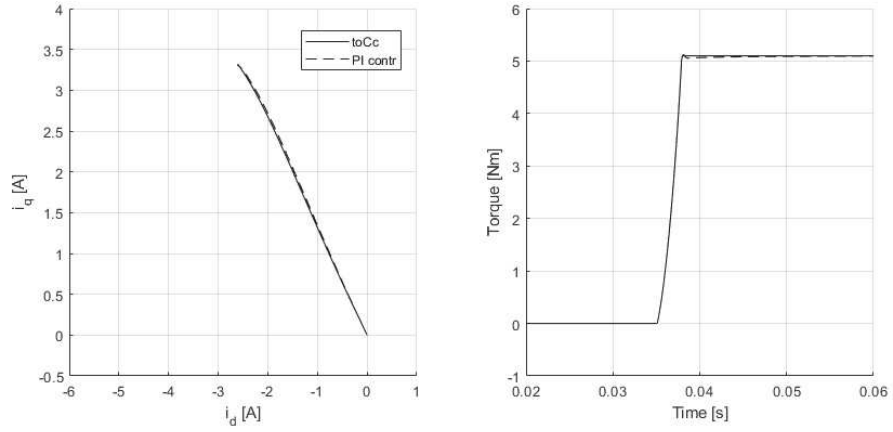

Figure 3.19: $i_d i_q$ frame and torque. Transient: $0 \leftarrow T_n, n_0 = 0$.

At zero speed, as seen in figure (3.19), the d- and q- axis are decoupled and both the controls produced roughly the same output.

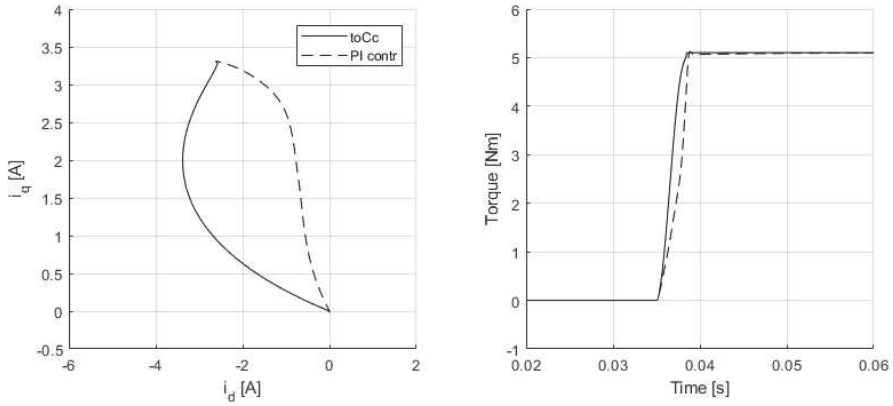

Figure 3.20: $i_d i_q$ frame and torque. Transient: $0 \leftarrow T_n, n_0 = 750\ rpm$.

Raising the speed to 750 rpm, as reported in figure (3.20), yields a variation of the currents paths in $i_d i_q$ frame, resulting in the *toCc* transient greater speed. Rising even more the rotor speed renders more pronounced the divergence of the two controllers, as seen in the figure below.

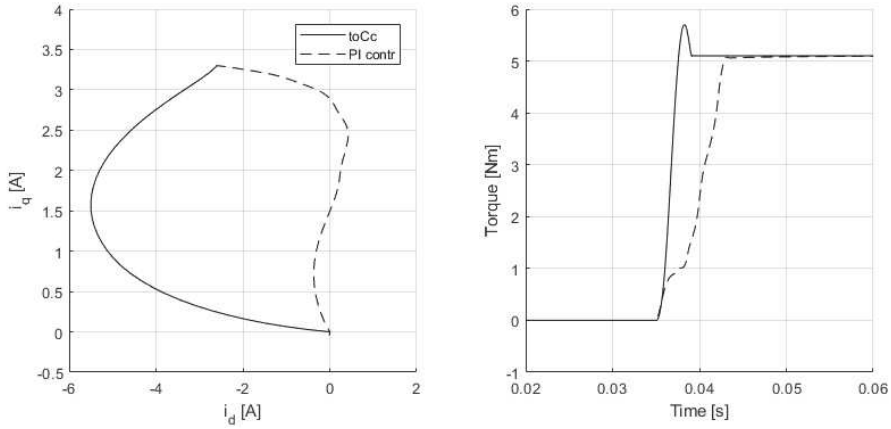

Figure 3.21: $i_d i_q$ frame and torque. Transient: $0 \leftarrow T_n, n_0 = 1500\ rpm$.

Noticeable is the peak that forms in the current i_d, which reaches a peak of 3 A over the target current. such high values of current can demagnetize the internal permanent magnets in the rotor, if grater currents are to be imposed.

Chapter 4

Speed control

In this chapter of the thesis it will be presented the attempt to combine the *toCc* with a traditional speed control, in order to obtain a faster rotor speed variation of the motor.

4.1 PI speed control

Using as base the control implemented in the previous two chapters, it has been realized the speed control. The control about to be realized, must be adapted to the current loop transfer function which in closed loop can be approximated as:

$$W(s) = \frac{1}{1 + \frac{s}{w_{c_i}}} \tag{4.1}$$

where w_{c_i} is the open loop zero crossing frequency of the open loop current control ($\cong$ 600 Hz). In light of this, the system to compensate has the following open loop transfer function:

$$H(s) = \frac{1}{1 + \frac{s}{w_{c_i}}} \cdot \frac{1}{B + sJ} \tag{4.2}$$

where B and J are respectively the air friction and inertia coefficients, which have value $B = 3.3e-2\ Nms$ and $J = 1.8e-4\ kg \cdot m^2$.
As the PI current control, the speed regulator has the following transfer function:

$$R_w(s) = k_{i_w} \frac{1 + sT_{PI_w}}{s}$$

To realize it, firstly it has been chosen the desired crossing frequency, which has been set at $w_{c_w} = 62,83\ rad/s$ ($\cong 10\ Hz$). Then it has been set $T_{PI_w} = B/J$ to compensate the pole introduced by the transfer function of the mechanical model. With the same procedure used with the PI current control it was obtain the following values:

- $k_{i_w} = 4.174$
- $k_{p_w} = 0.0226$

The bode diagram of the open loop transfer function $L_w(s) = R_w(s) \cdot H(s)$ becomes:

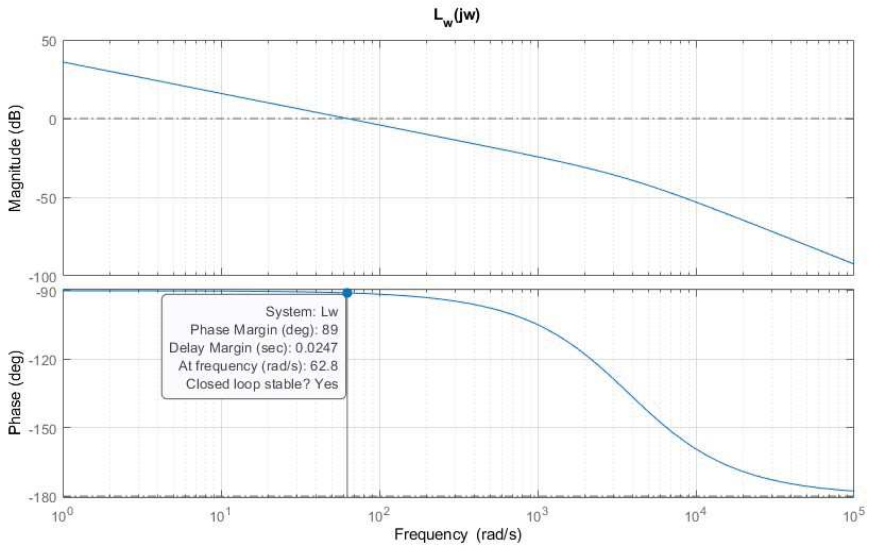

Figure 4.1: Magnitude and phase of the impulsive response $L_w(jw)$.

As indicated in figure (4.1) the system has the desired cross frequency, a phase margin $\varphi_m = 89°$ and, since it crosses the zero with a slope of $-20\ dB/dec$, the system is stable. If applied a step response from 0 to 500 rpm, the system yields the following response:

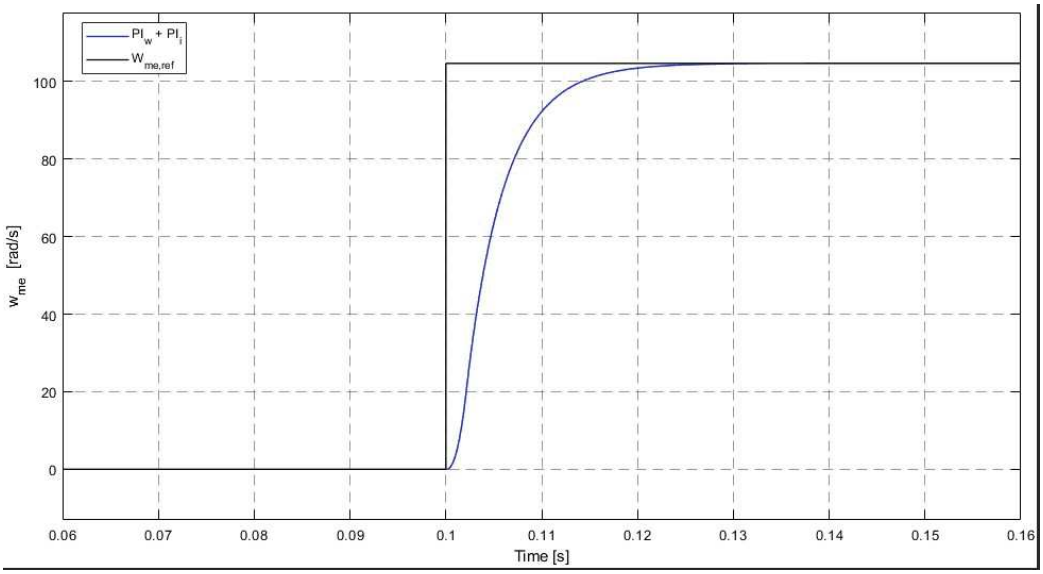

Figure 4.2: System response to the transient $0 \rightarrow n = 500\ rpm$ ($w_{me} \cong 105\ rad/s$).

As for the current control, it was implemented an anti-wind-up system for the speed regulator, which disables the integrative part of the regulator when the output current exceed the nominal one and limits it to that value.

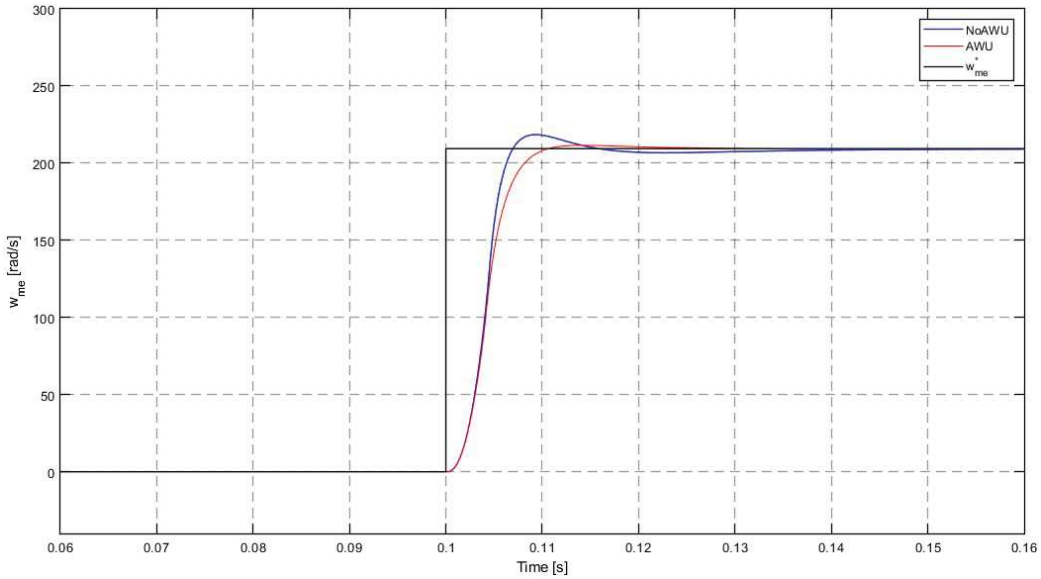

Figure 4.3: System response to the transient $0 \rightarrow n = 1000\ rpm$ ($w_{me} \cong 208\ rad/s$) with anti-wind-up and without.

4.2 PI regulator and *toCc* combination

After the speed regulator was implemented it has been tried together with *toCc*. The control was tested on the transients from 0 rpm to the target speeds: 500 rpm, 750 rpm, 1000 rpm, 1250 rpm and 1500 rpm. These are the results:

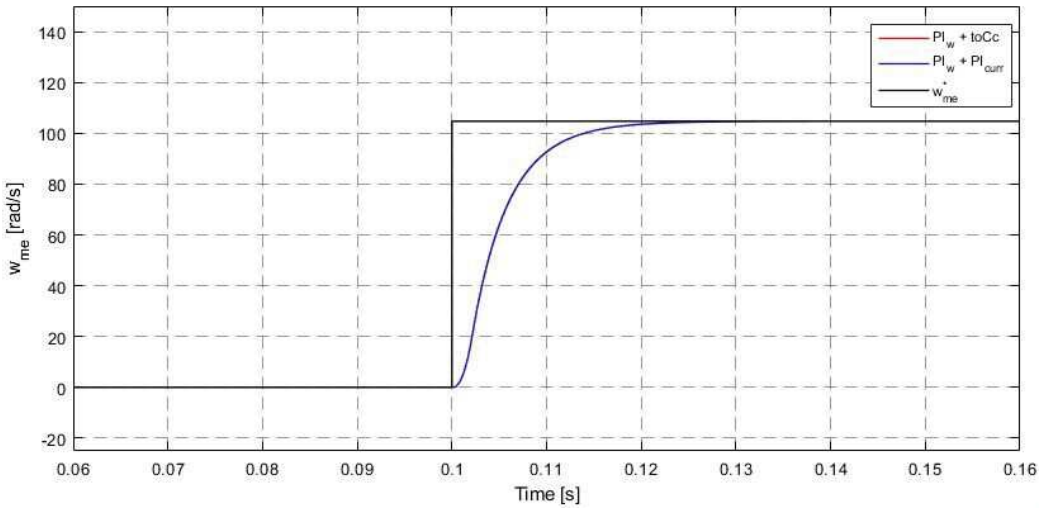

Figure 4.4: Speed transient $0 \rightarrow n = 500\ rpm$ ($w_{me} \cong 105\ rad/s$).

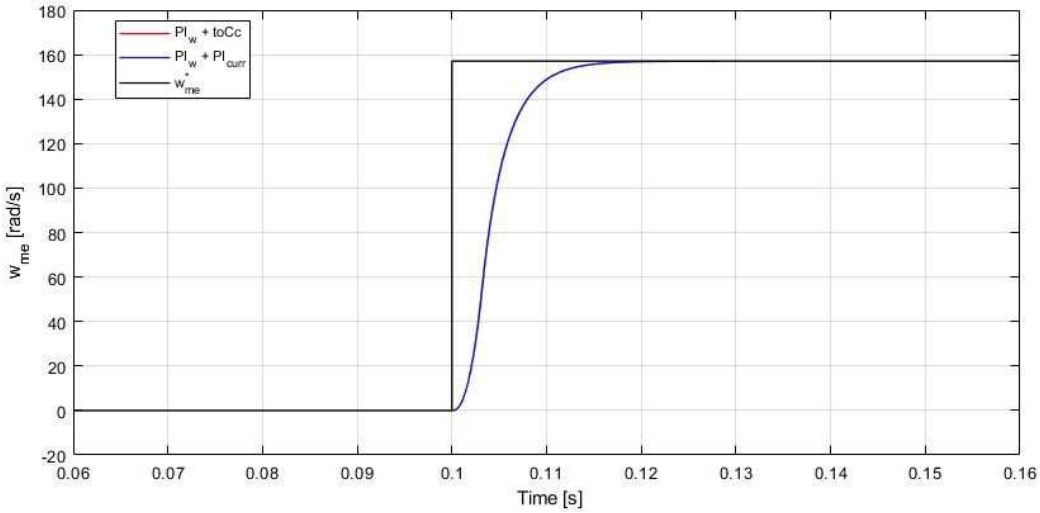

Figure 4.5: Speed transient $0 \rightarrow n = 750\ rpm$ ($w_{me} \cong 157\ rad/s$).

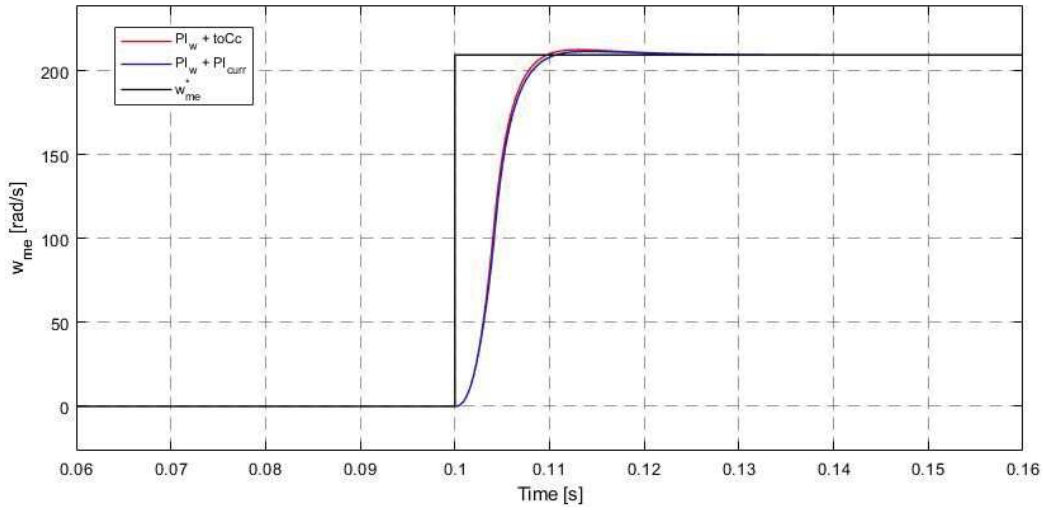

Figure 4.6: Speed transient $0 \rightarrow n = 1000\ rpm$ ($w_{me} \cong 208\ rad/s$).

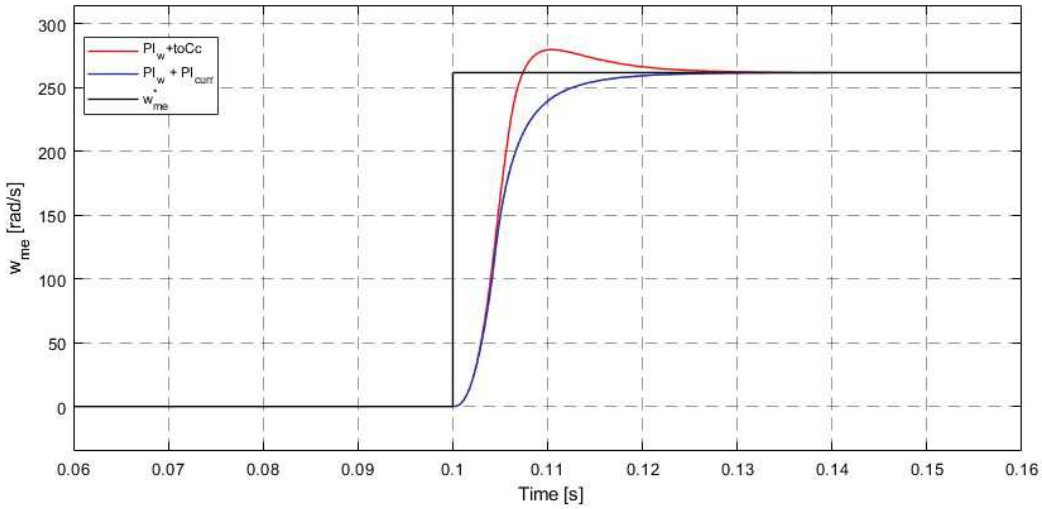

Figure 4.7: Speed transient $0 \rightarrow n = 1250\ rpm$ ($w_{me} \cong 262\ rad/s$).

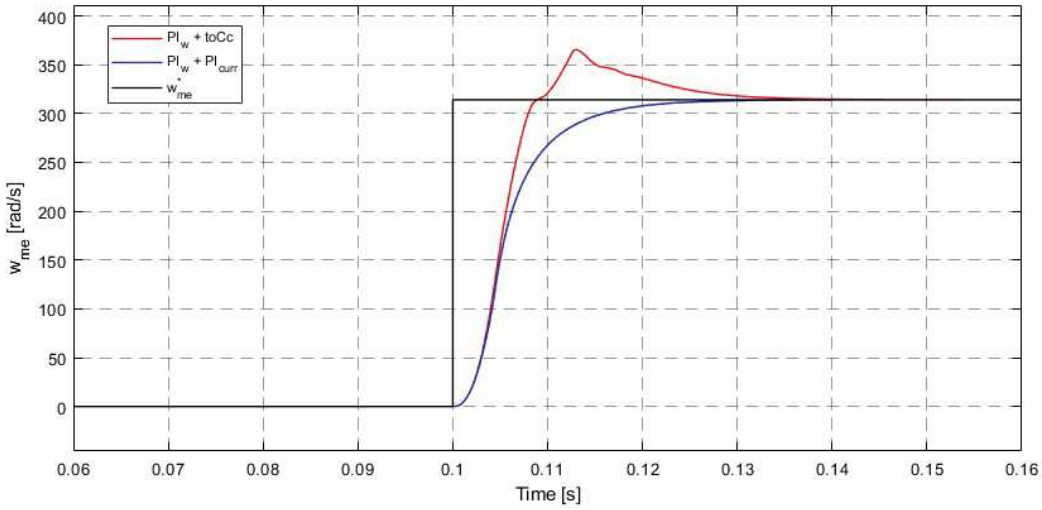

Figure 4.8: Speed transient $0 \rightarrow n = 1500\ rpm$ ($w_{me} \cong 314\ rad/s$).

Looking at the transients presented it can be seen that the effect of the *toCc* is noticeable only at high speeds, while at lower ones its influence is practically non-existent. This seems to be linked to the saturation of the speed regulator's output current.

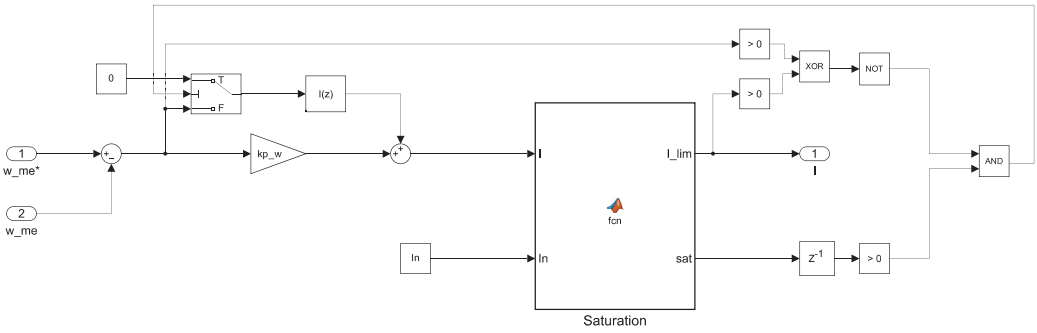

Figure 4.9: PI speed block view.

4.3 Speed control improvement

In this section will be discussed a way to improve the speed transient of the system at lower rotor speeds.

4.3.1 Error range

The first expedient uses an error threshold around the target speed, outside which it is forced the nominal current.

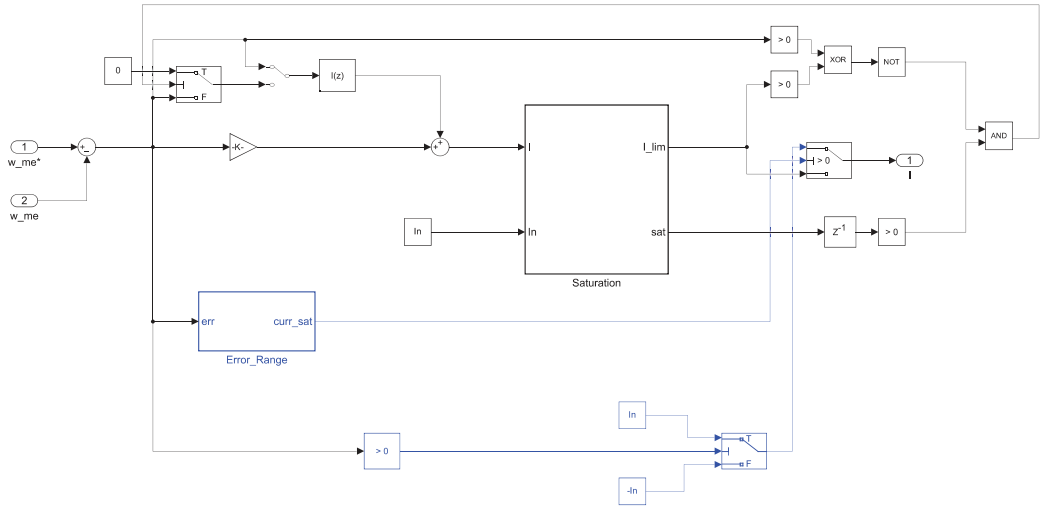

Figure 4.10: First attempt to improve speed transient.

In figure (4.10) it is highlighted the part that implements the control variation. The block `Error_Range`, in particular, outputs a logic value `curr_sat` that is equal to 1 when the error speed is higher then 10 rad/s, which selects I_n or $-I_n$ depending on the sign of the error.
The modification applied yielded the following results:

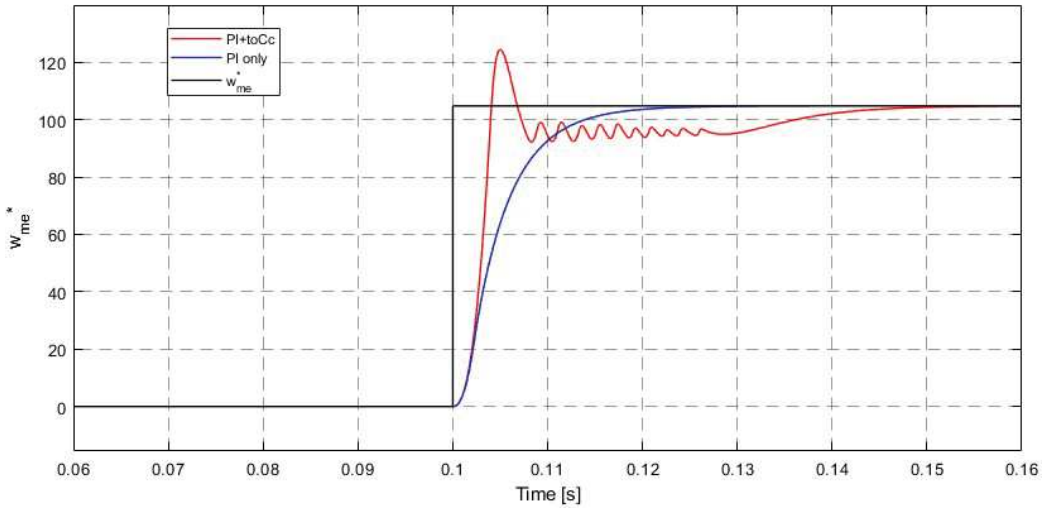

Figure 4.11: Speed transient $0 \rightarrow n = 500\ rpm$ ($w_{me} \cong 105\ rad/s$).

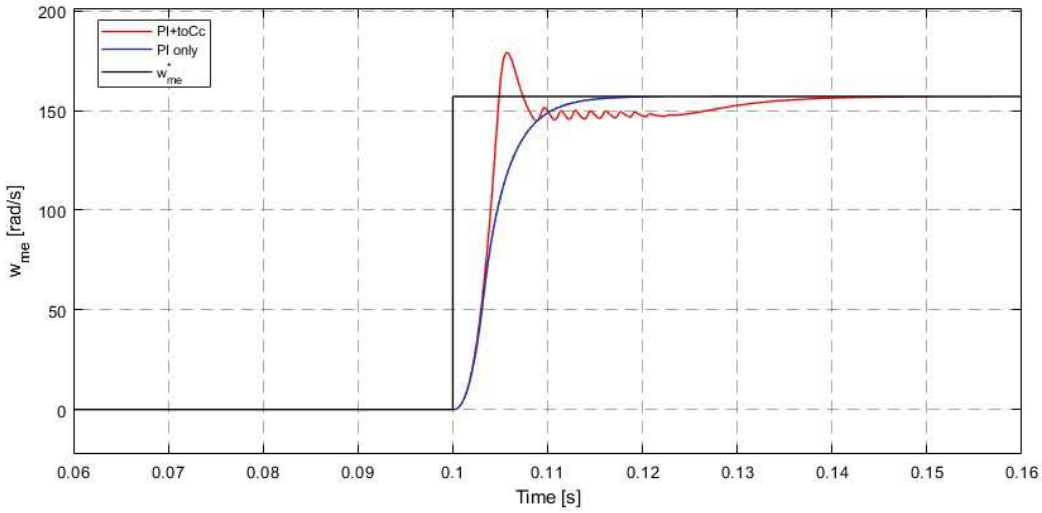

Figure 4.12: Speed transient $0 \rightarrow n = 750\ rpm$ ($w_{me} \cong 157\ rad/s$).

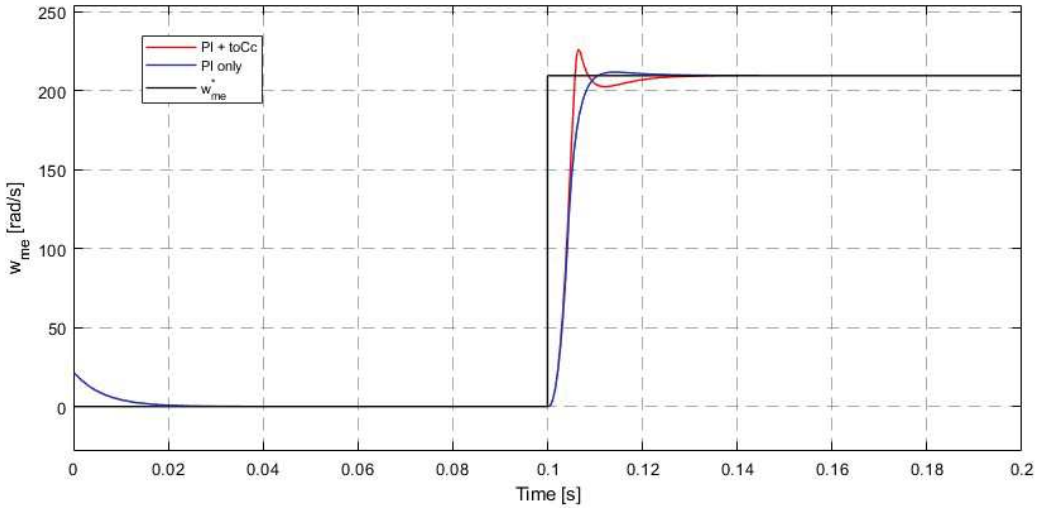

Figure 4.13: Speed transient $0 \rightarrow n = 1000\ rpm$ ($w_{me} \cong 208\ rad/s$).

Looking at the plots above it can be noticed an improvement in the speed transient, which becomes quicker if used with the *toCc*.
However the new control introduces an oscillation around lower limit of the error range, which is caused by the too low value of k_{p_w}, and by the integrative part of the control which is too low, due to rapid transient. The combination of the two, lowers the current output of the control, which lowers the speed and increases the speed error. Once it becomes higher than the limit imposed, the current is forced again to the nominal value. This cycle continues until the integrative part is high enough to maintain the error inside the imposed limit.
The new control strategy didn't provide the desired results.

4.3.2 Adaptive PI speed control

An other strategy was implemented to obtain a better transient. In the previous attempt, when the error was grater than the assigned value, the regulator didn't control the output current. During such period it doesn't matter if the PI control is stable and this can be used as an advantage. One problem of the speed regulator, in fact, is the too low value of k_{p_w}, which impresses a too low current to the current control. The value of the proportional constant could be increased in order to force a greater current out of the speed regulator, in order to increase the transient time where the *toCc* control works. Then it should reduce in the proximity of the desired speed.

To realize such control it has been used an *Adaptive PI speed control*, which varies the proportional constant with the value of the speed error, according to the expression:

$$k_{p_{w,mod}} = k_{p_w} \cdot \left[1 + \left(\frac{e_w}{\varepsilon_w}\right)^2\right] \tag{4.3}$$

where e_w is the speed error and ε_w is the error threshold, over which the proportional constant retains its original value.

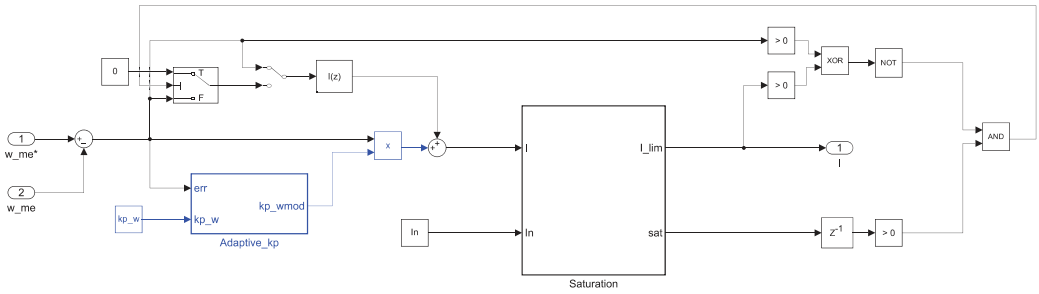

Figure 4.14: PI speed regulator block view with adaptive k_{p_w}.

Figure (4.14) shows the adaptive control implemented and in particular the block `Adaptive_kp` contains the expression 4.3, in which ε_w was given value 10 rad/s.
The graphs of the simulations are the following:

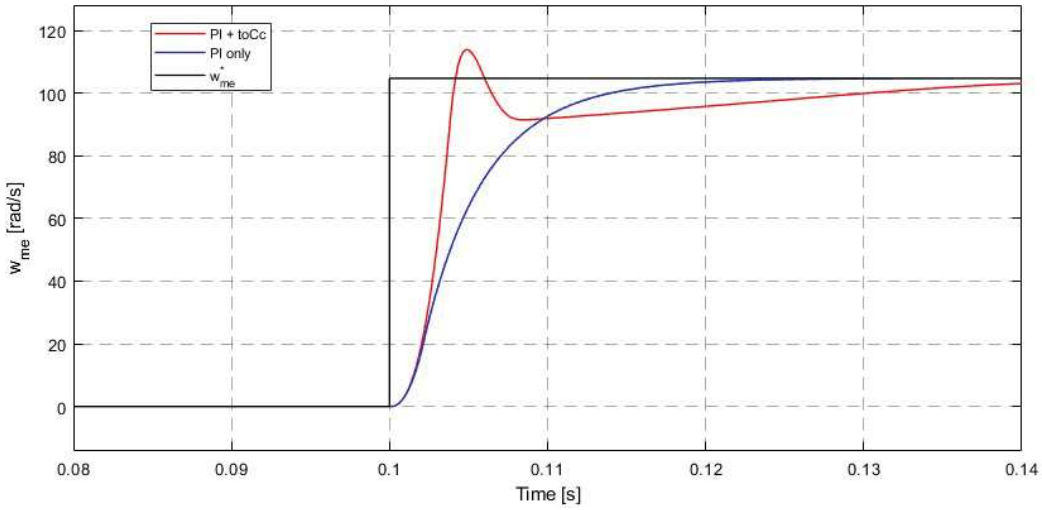

Figure 4.15: Speed transient $0 \rightarrow n = 500\ rpm$ ($w_{me} \cong 105\ rad/s$).

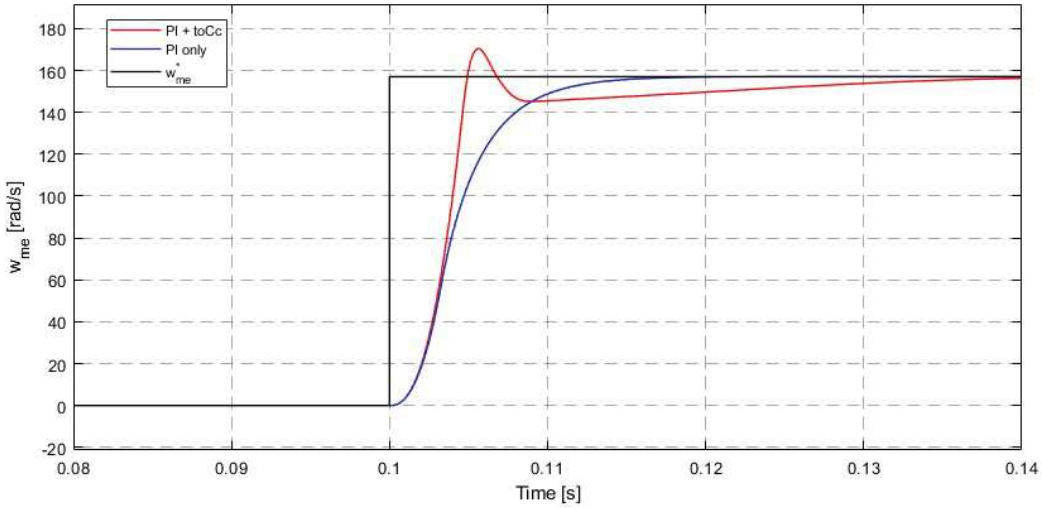

Figure 4.16: Speed transient $0 \rightarrow n = 750\ rpm$ ($w_{me} \cong 157\ rad/s$).

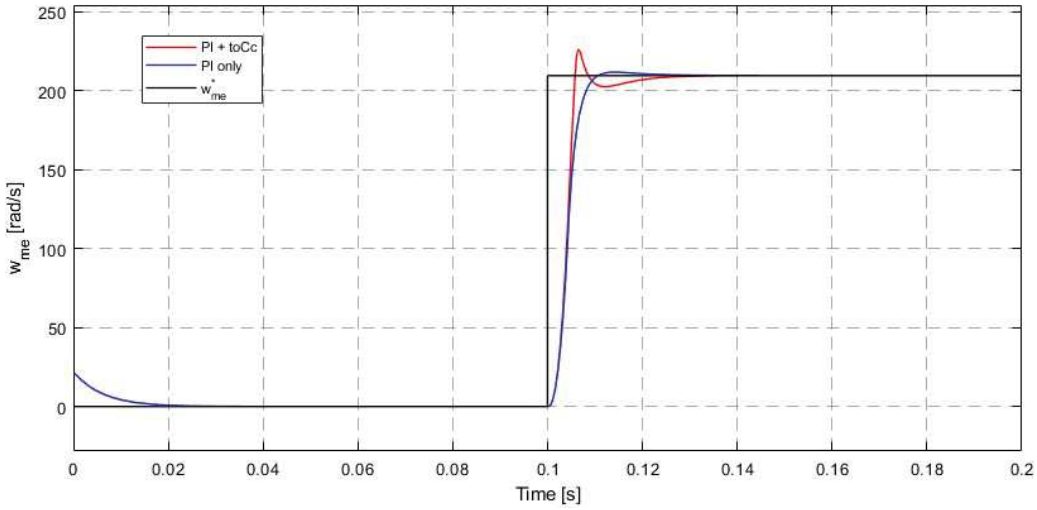

Figure 4.17: Speed transient $0 \rightarrow n = 1000\ rpm$ ($w_{me} \cong 208\ rad/s$).

As can be seen in the graphs above, the transients are similar to the ones shown in the previous paragraph, but without the oscillations around the error threshold.
Thanks to this expedient, the speed transients are consistently shorter in time than the ones which use the standard PI control on both speed and current control loops.

Bibliography

[1] Frank L. Lewis and Vassilis L. Syrmos, 1995, *Optimal Control*, US, Wiley-Interscience.

[2] Tommasini Matteo, *Innovative control algorithms for electric drives: Time Optimal Current and Torque Control of IPM SM Drives and Experimental Rig to test a Rotor Anisotropy-Based Sensorless Vector Control of IM Drives*[Phd Thesis]. Padova: Università degli studi di Padova, 2007.